Earth-Science Reviews 174 (2017) 1–21

Contents lists available at ScienceDirect

Earth-Science Reviews

journal homepage: www.elsevier.com/locate/earscirev

Sulfur and carbon isotopic evidence for metabolic pathway evolution and a four-stepped Earth system progression across the Archean and Paleoproterozoic

Jeff R. Havig[a,*], Trinity L. Hamilton[b], Aviv Bachan[a,1], Lee R. Kump[a]

[a] Department of Geosciences, Penn State Astrobiology Research Center, The Pennsylvania State University, University Park, PA 16802, USA
[b] Department of Plant and Microbe Biology, University of Minnesota, St. Paul, MN 55108, USA

ARTICLE INFO

Keywords:
Sulfur isotopes
Carbon isotopes
Archean
Paleoproterozoic
Metabolic pathways
Early earth
Great oxidation event

ABSTRACT

The Earth's mantle has provided a ready redox gradient of sulfur compounds (SO_2, H_2S) since the stabilization of the crust and formation of the ocean over 4 billion years ago, and life has evolved a multitude of metabolic pathways to take advantage of this gradient. These transitions are recorded in the sulfur and carbon isotope signals preserved in the rock record, in the genomic records of extant microorganisms, and in the changing mantle and crust structure, composition and cycling. Here, we have assembled approximately 20,000 sulfur ($\delta^{34}S$, $\Delta^{33}S$, $\Delta^{36}S$) and carbon ($\delta^{13}C$) isotope data points from scientific publications spanning over five decades of geochemical analyses on rocks deposited from 4.0 to 1.5 Ga. We place these data in the context of molecular clock and tectonic and surface redox indicators to identify overarching trends and integrate them into a holistic narrative on the transition of the Earth's surface towards more oxidizing conditions. The greatest extreme in $\delta^{34}S$ values of sulfide minerals (− 45.5 to 54.9‰) and sulfate minerals (− 13.6 to 46.6‰) as well as $\delta^{13}C$ values in carbonate minerals (− 16.8 to 29.6‰) occurred in the period following the Great Oxidation Event (GOE), while the greatest extremes in organic carbon $\delta^{13}C$ values (− 60.9 to 2.4‰) and sulfide and sulfate mineral $\Delta^{33}S$ and $\Delta^{36}S$ values (− 4.0 to 14.3‰ and − 12.3 to 3.2‰, respectively) occurred prior to the GOE. From our observations, we divide transitions in Earth's history into four periods: Period 1 (4.00 to 2.80 Ga) during which geochemical cycles were initialized, Period 2 (2.80 to 2.45 Ga) during which S and C isotope systems exhibit changes as conditions build up to the GOE, Period 3 (2.45 to 2.00 Ga) encompassing the GOE, and Period 4 (after 2.00 Ga) after which S and C isotopic systems remained relatively constant marking a time of Earth system geochemical quiescence. Using these periods, we link changes in S and C isotopes to molecular clock work to aid in interpreting emerging metabolic functions throughout Earth's history while underscoring the need for better proxies for robust evolutionary analyses. Specifically, results indicate: 1) an early development of sulfide oxidation and dissimilatory sulfite reduction followed by disproportionation and then sulfate reduction to sulfite resulting in a fully biologically mediated sulfur cycle by ~3.25 Ga; 2) support for the acetyl coenzyme-A pathway as the most likely earliest form of biologically mediated carbon fixation following methanogenesis; 3) an increasingly redox-stratified ocean in the Neoarchean with largely oxic surface water and euxinic bottom water during the first half of the Paleoproterozoic; and 4) that secular changes in Earth system crustal cycling dynamics and continent formation likely played a key role in driving the timing of the GOE. Finally, based on geochemical data, we suggest that the Paleoproterozoic be divided into a new Era of the Eoproterozoic (from 2.45 to 2.00 Ga) and the Paleoproterozoic (from 2.00 to 1.60 Ga).

1. Introduction

Microbial life gains energy and converts inorganic carbon into organic molecules through the use of sunlight (phototrophy) or chemical reactions (chemotrophy) that take advantage of redox reactions. Sulfur exhibits a wide range of oxidation states (from + 6 to − 2), and is released from the mantle via volcanism predominantly as SO_2 (+ 4) and H_2S (− 2). Sulfur released via subaerial volcanism is predominantly in the form of SO_2, while sulfur released in the subsurface can react with volcanic gases containing H_2 to form H_2S (Table 1). As such, the

* Corresponding author at: Department of Earth Sciences, University of Minnesota, Minneapolis, MN 55455, USA.
E-mail address: jhavig@umn.edu (J.R. Havig).
[1] Present address: Department of Geosciences, Stanford University, Stanford, CA.

http://dx.doi.org/10.1016/j.earscirev.2017.06.014
Received 17 November 2016; Received in revised form 21 June 2017; Accepted 29 June 2017
Available online 30 June 2017

Table 1
Relevant sulfur metabolisms and reactions, with $\delta^{34}S$ fractionations given, when known. Data compiled from Fry et al. (1985, 1986, 1988); Thompson et al. (1990); Fuseler et al. (1996); Janssen et al. (1996); Cypionka et al. (1998); Habicht et al. (1998); Böttcher et al. (2005); Canfield (2001); Machel (2001); Brunner and Bernasconi (2005); Holland (2009), and Poser et al. (2014). ATP = adenosine triphosphate, APS = adenosine 5′-phosphosulfate, AMP = adenosine monophosphate.

Metabolic pathway disproportionation	$\delta^{34}S$ Fractionation (relative to source, when known)
$2\ S^0 + 4\ H_2O \rightarrow 3\ H_2S + SO_4^{2-} + 2\ H^+$	Sulfide = –15.5 to –3.7 ‰, Sulfate = 10.9 to 30.9 ‰
$S_2O_3^{2-} + H_2O \rightarrow SO_4^{2-} + HS^- + H^+$	Sulfide = –20.4 to – 3 ‰, Sulfate = 1 to 14.4 ‰
$4\ SO_3^{2-} + H^+ \rightarrow 3\ SO_4^{2-} + HS^-$	Sulfide = –45.2 to –20.5 ‰, Sulfate = 6.9 to 12 ‰
Biological sulfate reduction (BSR)	Sum sulfide = –78 ‰ (max.)
1) $SO_4^{2-} + ATP \rightleftharpoons APS \rightleftharpoons AMP + SO_3^{2-}$	Sulfite = –25 ‰ (maximum)
2) $6\ H^+ + 3\ SO_3^{2-} \rightleftharpoons S_3O_6^{2-} + 4\ H_2O$ $S_3O_6^{2-} \rightleftharpoons S_2O_3^{2-} + \{SO_3^{2-}\}$ $S_2O_3^{2-} + 2\ H^+ \rightleftharpoons H_2S + \{SO_3^{2-}\}$ (Sulfite recycled)	Sulfide = –53 ‰ (maximum)
Anoxygenic photosynthesis	
$2\ H_2S + 3\ H_2O + h\nu \rightarrow S_2O_3^{2-} + 5\ H_2$	(No observed fractionation)
$CO_2 + 2\ H_2S + h\nu \rightarrow CH_2O + 2\ S^0 + H_2O$	Sulfur = 1 to 3 ‰
$3\ CO_2 + 2\ S^0 + 5\ H_2O + h\nu \rightarrow 3\ CH_2O + 2\ H_2SO_4$	(No observed fractionation)
Biological sulfide oxidation	
$2\ H_2S + O_2 \rightarrow 2\ S^0 + 2\ H_2O$	Sulfur = –4.1 to 1 ‰
$H_2S + 2\ O_2 \rightarrow H_2SO_4$	Sulfate = –5.1 to 18 ‰
$HS^- + 8\ H_2O \rightarrow SO_4^{2-} + 8\ H^+$ (anaerobic)	
via sulfide:quinone oxidoreductase pathway (SQR)	Sulfate = –4.3 to –1.3 ‰
via sulfur oxidation pathway (Sox)	Sulfate = –2.9 to –1.6 ‰
Abiotic processes	
Photolysis of SO_2 (in the atmosphere, with ultraviolet radiation)	
$3\ SO_2 + h\nu \rightarrow 2\ SO_3 + S^0$	(No observed mass-dependent fractionation)
Abiotic oxidation of sulfide	
$H_2S \rightarrow S^0, S_2O_3^{2-}, H_2SO_4$	Products = 4 to 5 ‰
Interaction of SO_2 with H_2 (cooling of volcanic gases in the subsurface)	
$SO_2 + 3\ H_2 \rightarrow H_2S + 2\ H_2O$	(No observed fractionation)
Thermochemical sulfate reduction (T > 100 °C, coupled to Fe or organic C oxidation)	
$H_2SO_4 \rightarrow SO_3^{2-}, S_2O_3^{2-}, S^0 \rightarrow H_2S$	(No observed fractionation)

potential simultaneous delivery of sulfur in two different redox states from the mantle has provided a ready sulfur redox gradient across all of earth history. In addition, life has evolved multiple metabolic pathways to exploit a wide range of sulfur compounds for generating energy (e.g., McCollom and Shock, 1997; Shock et al., 2005; Sleep and Bird, 2007). These metabolic pathways likely played an important role in the progressive oxidation of the earth's surface, and in resulting geochemical and geologic signals of this progression in the rock record (Kasting, 2013). Sulfur-coupled metabolisms are some of the most important microbially mediated processes, and are either directly or indirectly linked with carbon-coupled metabolisms, with both modifying redox conditions on Earth's surface. The rock record, while incomplete, provides our best framework for understanding the redox history of the Earth's surface (e.g, Farquhar et al., 2001; Hannisdal and Peters, 2011; Halevy, 2013), with isotopes of sulfur (including the mass independent fractionation of sulfur, or MIF-S signal) and carbon isotopes providing convincing evidence for the timing of the transition from an oxygen depleted/reducing atmosphere to one with free oxygen.

The isotopic values of carbon and sulfur recovered over the time period exhibit wide ranges. Sulfide mineral $\delta^{34}S$ values span a minimum of − 45.5‰ (at ~2.40 Ga) to a maximum of 54.9‰ (at ~2.09 Ga), while sulfate mineral $\delta^{34}S$ values span a minimum of − 13.6‰ (at ~2.43 Ga) to a maximum of 46.6‰ (at ~2.05 Ga). These values, however, are muted compared to extreme $\delta^{34}S$ values found in more recent units such as sulfide minerals ranging from − 72‰ in sediments overlying mid ocean ridge basalts (Lever et al., 2013) to 114.8‰ in pyrites enriched by microorganisms that couple sulfate reduction to anaerobic oxidation of methane (Lin et al., 2016); or sulfate $\delta^{34}S$ values of 135‰ in interstitial pore waters from ocean drilling cores as a result of slow sulfate reduction rates in low sulfate concentration environments (Rudnicki et al., 2001). Organic carbon $\delta^{13}C$ values ranged from a minimum of − 60.9‰ (at ~2.75 Ga) to a maximum of − 4.6‰ (at ~2.07 Ga), while carbonate $\delta^{13}C$ values ranged from a minimum of − 18.5‰ (at ~1.60 Ga) to a maximum of 29.6‰ (at ~2.10 Ga). As with sulfur, these rock values are muted compared to extremes measured in more recent samples. Methanotrophic biomass

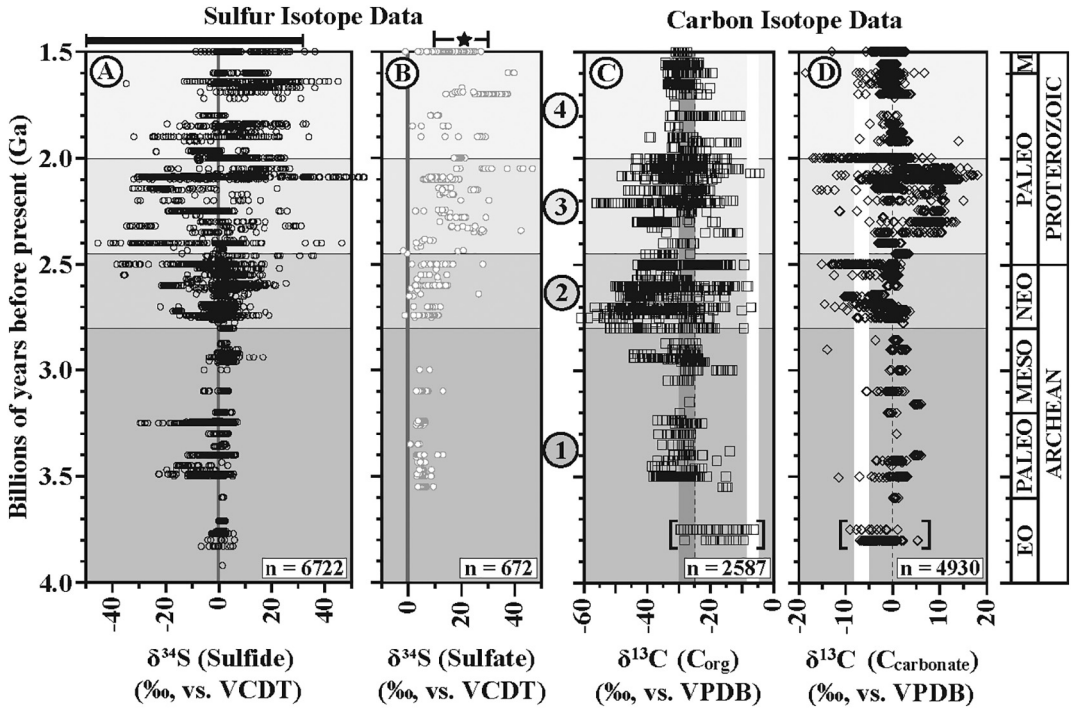

Fig. 1. Sulfur and carbon isotope data plotted against time, as compiled from literature for 1.5 to 4.0 Ga. Numbers of data points indicated in the lower right corner of plots. Horizontal demarcations for time Periods 1 through 4 are as described in text. A) Sulfide mineral $\delta^{34}S$ values. MORB $\delta^{34}S$ values indicated by a grey vertical bar (values from Labidi et al., 2012). Black horizontal bar at top shows range of modern values measured. B) Sulfate mineral $\delta^{34}S$ values. Grey vertical bar as described for A. Star indicates average value of the modern ocean sulfate pool (~21‰) and brackets show range of values from the Phanerozoic. C) Organic carbon $\delta^{13}C$ values. Modern bulk organic carbon values of −25‰ indicated with a vertical dashed line (Melezhik et al., 2013), and a range of −25 to −30‰ marked with a grey vertical bar (Hayes et al., 1999). Mantle $\delta^{13}C$ values of −8 to −5‰ are marked with a white vertical bar (Exley et al., 1986; Javoy et al., 1986; Deines, 2002; Horita and Polyakov, 2015). Samples from the Greenland Isua Greenstone Belt are bracketed. D) Inorganic carbon $\delta^{13}C$ values. Modern inorganic carbon value of 0‰ indicated by a dashed vertical line. Mantle $\delta^{13}C$ values of −8 to −5‰ are marked with a white vertical bar. Samples from the Greenland Isua Greenstone Belt are bracketed.

has been measured at $\delta^{13}C$ values as low as −85‰, while natural cyanobacterial biomass has been measured at values as high as −3‰, and methanogenic biomass as high as 6‰ (Schidlowski, 2001). Carbonate $\delta^{13}C$ values have been documented at values as low as −125‰ from deposition from carbon-poor groundwater related to sulfate-dependent anaerobic methane oxidation (Drake et al., 2015) and as high as 34‰ in cements associated with dissolved inorganic carbon influenced by methanogenesis (Budai et al., 2002). Given these wide ranges that have been found to date associated with the complex systematics of sulfur and carbon isotope fractionations and distillations, it is imperative that we interpret rock record values carefully and consider the ranges of values that we can associate directly to known metabolic pathways (e.g., carbon fixation pathways, biological sulfate reduction, microbially mediated disproportionation, etc.) measured from pure culture experimental work.

By merging comprehensive geochemical datasets from the literature with our current understanding of microbial sulfur and carbon transformations, we can better constrain the onset of the biological innovations. To do so, we draw on three lines of evidence: *i*) sulfur and carbon major stable isotope data, *ii*) geochemical contextual evidence for progressive though not necessarily linear (e.g., Kump, 2008; Lyons et al., 2014; Gumsley et al., 2017) oxidation of the earth's surface, including the sulfur isotope mass-independent fractionation (MIF-S) signal recorded in the rock record, and *iii*) the microbial metabolic machinery recorded in the genomic record of extant life and the isotopic signals they generate.

First we present sulfur and carbon stable isotope data, summarizing background information on each isotope system as it relates to global surface redox and describing trends observed from data compiled from the literature. Next we discuss the connection between microbial metabolism and sulfur compounds, followed by a section that lays out the relationship between carbon fixation metabolisms and the carbon isotope system, and then a brief treatment of molecular clock calculations. Other select information from the rock record that relate to the oxidation of the Earth's surface and the Great Oxidation Event (GOE) are briefly described in the Rock Record Contextual Information section. Finally, we provide a synthesis of all the geochemical, biological, and geologic information in four time periods: Period 1: 4.0 to 2.8 Ga-the beginnings of modern Earth system dynamics, with relatively small differences between $\delta^{34}S$ values of sulfide and sulfate minerals (Fig. 1A, B), organic carbon $\delta^{13}C$ values that range between −13.1 and −44.3‰ (Fig. 1C), carbonate $\delta^{13}C$ values near 0‰ (Fig. 1D), and $\Delta^{33}S$ and $\Delta^{36}S$ values of sulfides and sulfates contain mass independent fractionation signals (Fig. 2A, B); Period 2: 2.8 to 2.45 Ga-the buildup to the GOE), where we observe an expansion in the range of sulfide and sulfate mineral $\delta^{34}S$ values (Fig. 1A, B) as well as $\Delta^{33}S$ and $\Delta^{36}S$ values (Fig. 2A, B), an increase in occurrence of more negative $\delta^{13}C$ values in both organic carbon (minimum of −60.9‰) and carbonate minerals (minimum of −15.0‰) (Fig. 1C, D); Period 3: 2.45 to 2.0 Ga-The GOE, characterized by a further expansion in the range in $\delta^{34}S$ values in both sulfide and sulfate minerals (Fig. 1A, B), a collapse in the $\Delta^{33}S$ and $\Delta^{36}S$ values in both sulfide and sulfate minerals (Fig. 2A, B), and a shift towards positive $\delta^{13}C$ values in both organic carbon and carbonate minerals (Fig. 1C, D); and Period 4: after 2.0 Ga-Earth system quiescence, when sulfide mineral $\delta^{34}S$ values trend to the positive (Fig. 1A), and the ranges of organic carbon and carbonate mineral $\delta^{13}C$ values decrease dramatically (Fig. 1C, D).

2. Sulfur and carbon stable isotope data

Carbon is present as two stable isotopes, ^{12}C and ^{13}C, with ^{12}C accounting for 98.93%, and ^{13}C for 1.07%. Sulfur is present as four stable isotopes, including ^{32}S (94.93%), ^{33}S (0.76%), ^{34}S (4.29%), and ^{36}S (0.02%). All isotopic data are reported as isotope ratios, relative to

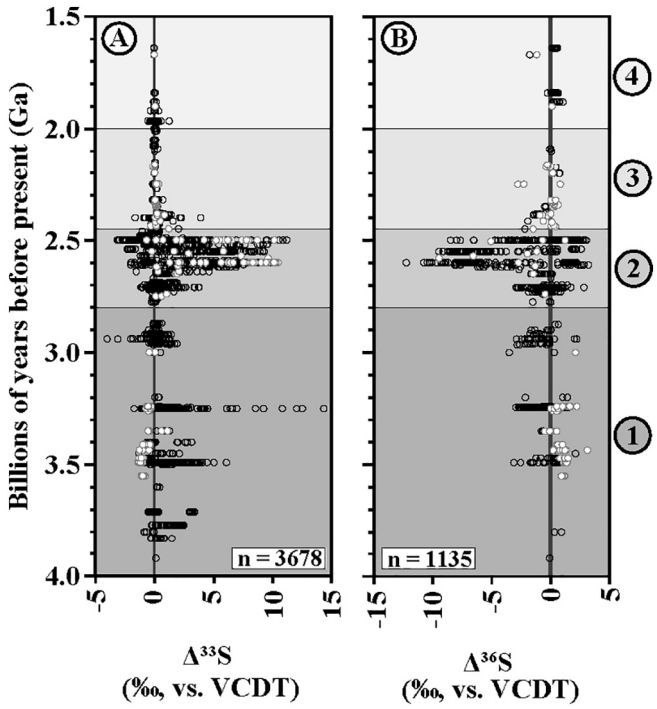

Fig. 2. Sulfur isotope data plotted against time, as compiled from literature for 1.5 to 4.0 Ga. Numbers of data points indicated in the lower right corner of plots. A) Sulfide (open black circles) and sulfate (white-filled grey circles) mineral $\Delta^{33}S$ values. MORB values indicated by a grey vertical bar (values from Labidi et al., 2012). B) Sulfide and sulfate mineral $\Delta^{36}S$ values, symbols and vertical grey bar as described for A. Horizontal demarcations for time Periods 1 through 4 are as described in text.

standards of known value, using the equation [(isotope ratio of sample) / (isotope ratio of standard) − 1] × 1000, expressed in delta notation (δ) and reported as per mil (‰). For sulfur, the standard is the Vienna Canyon Diablo Troilite (VCDT), based on troilite (an iron-sulfide mineral) found in the octahedrite iron meteorite that formed Barringer Crater in Arizona, USA approximately 50,000 years ago. Stable sulfur isotopes are reported as the ratio of the minor isotope (^{33}S, ^{34}S, or ^{36}S) to the major isotope (^{32}S), (e.g. $\delta^{34}S$ is [($^{34}S/^{32}S$ of sample) / ($^{34}S/^{32}S$ of standard) − 1] × 1000). For carbon, the standard is the Vienna Pee Dee Belemnite, based on the value of the marine fossil *Belemnitella americana* found in the Cretaceous Pee Dee Formation in South Carolina, USA. Stable carbon isotopes are reported as the ratio of the minor isotope (^{13}C) to the major isotope (^{12}C) as $\delta^{13}C$ (i.e. [($^{13}C/^{12}C$ of sample) / ($^{13}C/^{12}C$ of standard) − 1] × 1000).

An alternative form of isotope reporting uses the difference between a measured isotopic value to that of an expected value. This has become the norm for reporting the minor isotopes of sulfur (^{33}S and ^{36}S) based on their deviation from the expected linear mass-dependent isotopic relationship of $\Delta^{33}S = \delta^{33}S - 0.515 \times \delta^{34}S$ and $\Delta^{36}S = \delta^{36}S - 1.90 \times \delta^{34}S$, given in the Δ, or 'capital delta' notation (Hulston and Thode, 1965).

We compiled carbon and sulfur isotopic data reported from 4.0 to 1.5 Ga that are available in publications through 2014. In total, 6722 sulfide $\delta^{34}S$ data points (Fig. 1A), 672 sulfate $\delta^{34}S$ data points (Fig. 1B), 2587 organic carbon $\delta^{13}C$ data points (Fig. 1C), and 4930 inorganic carbon (carbonate) $\delta^{13}C$ data points (Fig. 1D), as well as 3678 sulfide and sulfate $\Delta^{33}S$ data points (Fig. 2A) and 1135 sulfide and sulfate $\Delta^{36}S$ data points (Fig. 2B) are reported from literature sources. Individual analyses were included where possible, and estimated unit age dates based on confining units with age dates were used when the units were not directly age dated.

All reported data points were used. For interpretation, it is important to keep in mind that the raw data are not without their biases. Potential biases include: geographic bias (sampling focused on easily accessible sampling locations), preservation bias (most of the rock record has been destroyed, and the likelihood of annihilation and/or metamorphism increases with age), sedimentary bias (e.g., greater occurrence of preserved marginal, shallow water settings, dearth of deep marine setting preservation), temporal bias (increased sampling of certain time periods, usually coincident with extreme isotopic shifts), among others (Shields and Veizer, 2002). Differences in analysis method also impact the data. For instance, bulk analysis of entire pyrite grains or rocks containing multiple pyrite mineral grains homogenizes small scale variability between pyrite grains or within individual pyrite grains, losing the fidelity that is available through Secondary Ion Mass Spectrometry (SIMS) analyses. Furthermore, the numbers of data points produced from multiple small to nano-scale analyses (especially for multiple analyses of single pyrite grains via SIMS) can produce a large number of analyses that might be a single data point generated from a bulk technique. The data set presented here is, to the best of our knowledge, the largest openly available compilation of carbon and sulfur isotope data to date (available as SOM) and thus provides a foundation from which to interpret the rock record. However, we do not presume it to be all inclusive. One of the goals of this compilation is to provide a platform from which the scientific community can amend, build upon, and add to as new information becomes available.

Covarying trends across the isotopic systems reveal 4 distinct intervals (periods), each characterized by unique behaviors (Figs. 1 and 2). Period 1, from 4.00 to 2.80 Ga (covering the Eoarchean, Paleoarchean, and Mesoarchean), is characterized by isotopic signal quiescence. Period 2, from 2.80 to 2.45 Ga (encompassing the Neoarchean, and leading up to the shift from a reducing to an oxidizing atmosphere), exhibits the greatest spread in $\Delta^{33}S$ and $\Delta^{36}S$ values. Period 3, from 2.45 to 2.00 Ga (covering the first part of the Paleoproterozoic), which follows the switch of the atmosphere from anoxic to oxic and the Great Oxidation Event, is characterized by the collapse of the spread in $\Delta^{33}S$ and $\Delta^{36}S$ values and a large range in $\delta^{34}S$ and $\delta^{13}C$ values, including a protracted period of positive carbonate $\delta^{13}C$ isotopes. Period 4, from 2.00 to 1.50 Ga (including the second part of the Paleoproterozoic and the beginning of the Mesoproterozoic), is characterized by the decline of the large-scale variations in organic and inorganic $\delta^{13}C$ values recorded in periods 2 and 3, and a decrease in the spread of $\delta^{34}S$ values, all heralding the start of the 'boring billion' (1.80 to 0.80 Ga). Binning $\delta^{34}S$ and $\delta^{13}C$ values shows the overall progression of isotopic values through the four periods (Fig. 3). The majority of sulfide $\delta^{34}S$ values reported for Periods 1 and 2 fall close to mantle values. The greatest spread in values (with most values falling below mantle values) is observed during Period 3. Values predominantly greater than mantle values occur in Period 4. Nearly all sulfate $\delta^{34}S$ values fall above mantle values, and become progressively more positive through the four periods. Most organic carbon $\delta^{13}C$ values fall below − 25‰, and abruptly transition from less negative in Period 1 to predominantly more negative in Period 2, then becoming less negative through periods 3 and 4. Inorganic $\delta^{13}C$ values predominantly fall close to modern marine carbonate and dissolved inorganic carbon values (ca. 0‰). In Period 1 over 67% of analyses fall above 0‰, while in Period 2 there is an increase in the number of more negative inorganic $\delta^{13}C$ values (56% of values fall below 0‰), and in Period 3 while there are still many negative values reported, there is a larger number of positive values, with 65% > 0‰ and 36% > 5‰. In Period 4, nearly all carbonate $\delta^{13}C$ values collapse to around 0‰, though 68% fall below 0‰.

Isotopic signals recorded in the rock record (e.g., $\delta^{34}S$ and $\delta^{13}C$) are influenced by metabolic processes, making the basis of the four divisions driven in part by life. In the following two sections we present brief overviews of sulfur and carbon metabolisms for readers less familiar with them.

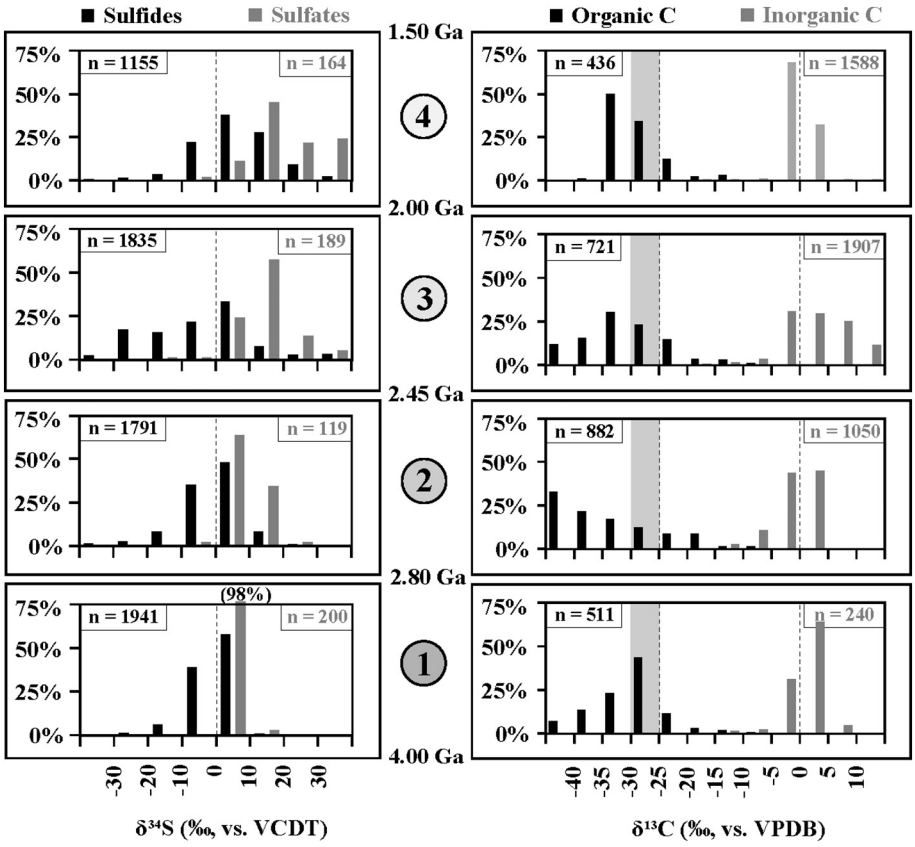

Fig. 3. Histograms for percentage of data points per bin for sulfide and sulfate mineral $\delta^{34}S$ values (left) and organic and inorganic carbon $\delta^{13}C$ values (right), with bin ranges defined by the x-axis. Reference $\delta^{34}S$ and $\delta^{13}C$ values as described in Fig. 1. Horizontal demarcations for time Periods 1 through 4 are as described in text. Isua Greenstone Belt samples were not included for the $T = 1$ $\delta^{13}C$ histogram.

3. Biology of S metabolisms

The wide range of oxidation states of sulfur (-2 to $+6$) provide many intermediates for biological oxidation, reduction, and disproportionation. The dissimilation of sulfur compounds may have been one of the earliest biological strategies for energy generation (e.g., Canfield and Raiswell, 1999; Canfield et al., 2006; Grein et al., 2013). Although sulfate concentrations were probably much lower during the Archaean (e.g., Habicht et al., 2002; Crowe et al., 2014; Jamieson et al., 2013), reduced sources of sulfur (H_2S, S^0) supplied from volcanic activity would have been readily available during this time, fueling biologically mediated sulfide, sulfur oxidation, and disproportionation of sulfur species as sources of energy for the microbiota. Biologically mediated sulfate reduction could have become a major source of sulfide following oxidation of the continents and the subsequent increase in marine sulfate concentrations although sulfite and thiosulfate would have been suitable electron acceptors prior to this increase (e.g., Halevy, 2013). We have compiled sulfur redox reactions discussed here along with measured fractionation factors reported in the literature (Table 1). This list represents most of the fundamental reactions which are best characterized, but it is not exhaustive. Examples we overlook include the disproportionation of thiosulfate to elemental sulfur and sulfite ($S_2O_3^{2-} => S^0 + SO_3^{2-}$) proposed by Cypionka et al. (1998), as well as the multiple intermediate steps in the biologically mediated oxidation of sulfide (e.g., Poser et al., 2014). Furthermore, the maximum values for BSR given in Table 1 (from Brunner and Bernasconi, 2005) are greater than the largest fractionation measured in pure culture experiments (66‰, Sim et al., 2011), but are similar to the maximum that has been measured in natural settings (75‰, Wortmann et al., 2001), indicating pure culture analyses may not always represent values that can be attained in natural settings.

Inorganic sulfur metabolism is extremely complicated due to the complex chemistry of sulfur (including multiple oxidation states) and the large number of enzymatic pathways that have evolved to utilize sulfur (Frigaard and Bryant, 2008). Today, the biogeochemical cycling of sulfur through these redox states is catalyzed by microorganisms and results in a broad range of sulfur isotope fractionation (Table 1). Sulfur oxidation is catalyzed by phylogenetically distinct and physiologically diverse bacteria including chemotrophic and phototrophic bacteria as well as the Sulfolobales (aerobic Archaea). These organisms oxidize a variety of reduced sulfur species including sulfide, elemental sulfur, and thiosulfate, producing elemental sulfur or sulfate as the end product. Organisms that use sulfate as an electron acceptor include members of Bacteria (Deltaproteobacteria, Clostridia, Thermodesulfobiaceae, Nitrospirae, Thermodesulfobacteria), members of the Crenarchaeota (Thermocladium, Caldivirga), and the Euryarchaeota (Archaeoglobus) (Muyzer and Stams, 2008), typically producing sulfide. In pure cultures, the use of other intermediate oxidation state sulfur compounds including sulfate reduction intermediates (e.g., sulfite or thiosulfate) has been observed (Price et al., 2014). Sulfate reducing organisms are also crucial to the carbon cycle as their activity accounts for a large portion of the remineralization of fixed carbon (oxidizing organic carbon to CO_2, and thereby returning it to the dissolved inorganic carbon or DIC pool), linking sulfate reducing organisms (SROs) to the precipitation of carbonate minerals from DIC as well as pyrites (through the generation of H_2S from sulfate reduction) through the generalized reaction: $SO_4^{2-} + 2\ CH_2O => H_2S + 2\ HCO_3^-$. The biochemical and genetic underpinnings of sulfur disproportionation are poorly understood but the process is carried out by a diverse array of microorganisms. In addition to these energy-yielding reactions, organisms encode the machinery necessary for uptake and assimilation of sulfate (assimilatory sulfate reduction) specifically for synthesis of macromolecules (i.e., proteins).

The sulfur oxidation enzyme system (Sox) has been identified in a number of organisms capable of oxidizing reduced sulfur compounds. Pure culture in vitro analyses indicate large substrate versatility by Sox including the oxidation of thiosulfate, sulfite, sulfur, and hydrogen sulfide (Rother et al., 2001). In the event that elemental sulfur is

formed, some organisms may store this intermediate intra- or extracellularly and further oxidize it to sulfate when more reduced electron donors such as sulfide or thiosulfate become limiting (Nelson and Castenholz, 1981; Schmidt et al., 1987). In *Acidianus ambivalens*, a member of the Sulfolobales, a sulfur oxygenate reductase (SOR) catalyzes sulfur disproportionation coupled to an oxygenate reaction (Sun et al., 2003; Kletzin et al., 2004) and a membrane-bound thiosulfate-quinone oxidoreductase (TQO) links thiosulfate consumption to oxygen reduction (Müller et al., 2004). Many organisms encode sulfide:quinone oxidoreductase (Sqr), a flavoprotein that oxidizes sulfide. Single genomes may encode multiple types of Sqrs (Marcia et al., 2010; Gregersen et al., 2011) although the precise physiological function of each type is still under investigation. Regardless, phylogenetic reconstruction of 16S rRNA gene sequences and *sqr* are not typically congruent, hindering interpretation of the evolutionary history of this protein. Flavocytochrome *c*, another flavoprotein, oxidizes sulfide in vitro while the function of this protein in vivo has not been demonstrated. Other proteins, including polysulfide reductase and rhodanese-related sulfurtransferases, have been implicated in sulfur oxidation but warrant further investigation to determine their phylogenetic distribution and contribution to the oxidation of reduced sulfur compounds.

Dissimilatory sulfate reduction occurs through a series of enzymatic reactions (Table 1). First, sulfate is activated by sulfate adenylyl transferase (Sat) forming adenosine-phosphosulfate (APS) which is reduced through the action of adenosine-5′-phosphosulfate (APS) resulting in sulfite (Muyzer and Stams, 2008). The reduction of sulfite to sulfide is catalyzed by dissimilatory sulfite reductase (DsrAB) (Rabus et al., 2007). Components of the Dsr system as well as the dissimilatory APS reductase genes (AprBA) are also employed by some sulfur oxidizing organisms albeit in the opposite (oxidative) direction (Frigaard and Dahl, 2009; Gregersen et al., 2011). Similarly, the enzymatic pathways of assimilatory and dissimilatory sulfate reduction both start with the activation of sulfate, a reaction catalyzed by sulfate adenylyl transferase (Sat) (Rabus et al., 2007; Frigaard and Dahl, 2009). In general, phylogenetic reconstructions indicate component enzymes cluster distinctly based on function—oxidation or reduction, assimilation or dissimilation—for instance. Unfortunately, evolutionary analyses of proposed gene duplication events resulting in the delineation between enzymes involved in the oxidative or reductive pathways is hindered by evidence for multiple gene transfer events (Boucher et al., 2003).

The complex chemistry of sulfur, the multitude of enzymatic machinery that has evolved to utilize sulfur species, and the cycling of intermediates (e.g., sulfite, thiosulfate) has implications on both the evolutionary history of these enzymes and the fractionation of S isotopes. Environmental factors (e.g., substrate concentration and type, temperature) and biological factors (e.g., metabolism rates, internal cycling of intermediates, interactions between different metabolisms, diel cycling) have been shown to influence the fractionation imparted on sulfide during sulfate reduction (e.g., Habicht and Canfield, 1997; Canfield, 2001). The isotopic signature imparted on sulfur through enzymatic reactions is difficult to interpret due to the range of oxidation states of sulfur and the numerous ways in which microorganisms cycle sulfur through intermediate redox states, and biologically mediated reactions could mask abiotic processes that may also contribute (Table 1). Notable progress has been made on deciphering S fractionation through some of these pathways—sulfate reduction for instance (e.g., Leavitt et al., 2013; Zhelezinskaia et al., 2014) and sulfide oxidation (e.g., Poser et al., 2014). We expect that further studies examining reduction and re-oxidation of sulfur compounds in situ such as Pellerin et al. (2015) will further enlighten S fractionation as a result of biogeochemical cycling and thus our interpretation of the rock record.

4. Biology of C metabolisms

Key early evolving carbon metabolisms include carbon fixation (conversion of inorganic C into organic C), methanogenesis (metabolisms that result in the production of CH_4), and fermentation (anaerobic breakdown of organic material). Carbon fixation allowed the conversion of oxidized carbon (as CO_2) into reduced carbon, and the burial of reduced organic carbon is one of the fundamental forces that helped drive the oxidation of the Earth's surface. Methanogenesis would have provided a chemotrophic means for gaining energy on early earth, and fermentation (a form of anaerobic heterotrophy) would have driven the breakdown of organic matter and release as CO_2, and both would have provided ready energy sources for early metabolisms through the release of a suite of reduced constituents (e.g., CH_4 from methanogenesis; H_2, acetate, methanol, ethanol, propionate, formate, lactate, etc. from fermentation). Below we discusses carbon fixation and its link to photosynthesis, methanogenesis, and fermentation, and how each can be connected to the carbon isotope signal in the rock record as parts of the global carbon cycle.

Table 2
Carbon fixation metabolisms with $\delta^{13}C$ fractionations for generated biomass given and characteristics of each metabolism (top) and fractionation factors for methane from the carbon source generated via methanogenesis (bottom). D4H = dicarboxylate-4-hydroxybutyrate Cycle, 3H4H = 3-hydroxyproprionate-4-hydroxybutyrate Cycle, rTCA - reductive Tricarboxylic Acid Cycle (Krebs Cycle, reversed citric acid cycle), 3HP = 3-hydroxypropionate bicycle, ACP = Acetyl-Coenzyme A Pathway (Wood-Ljungdahl Pathway), rPPC = reductive Pentose Phosphate Cycle (Calvin Cycle), H2 = hydrogenotrophic, Ac = acetoclastic, All = all methylotrophic pathway fractionations, MeOH = methanol, TMA = Trimethyl amine, DMS = dimethyl sulfide. *A fractionation factor has been reported of only −7‰ for acetoclastic methanogenesis (Valentine et al., 2004). Carbon Fixation sources: Sirevåg et al. (1977); Quandt et al. (1977); Holo and Sirevåg (1986); Fuchs et al. (1979); Preuß et al. (1989); Ivanovsky et al. (1993); van der Meer et al. (2001); House et al. (2003); McNevin et al. (2007); Berg et al. (2010); Bar-Even et al. (2011); and Havig et al. (2011). Methanogenesis sources: Horita and Berndt (1999); Whiticar (1999); Valentine et al. (2004); Conrad (2005); and Londry et al. (2008).

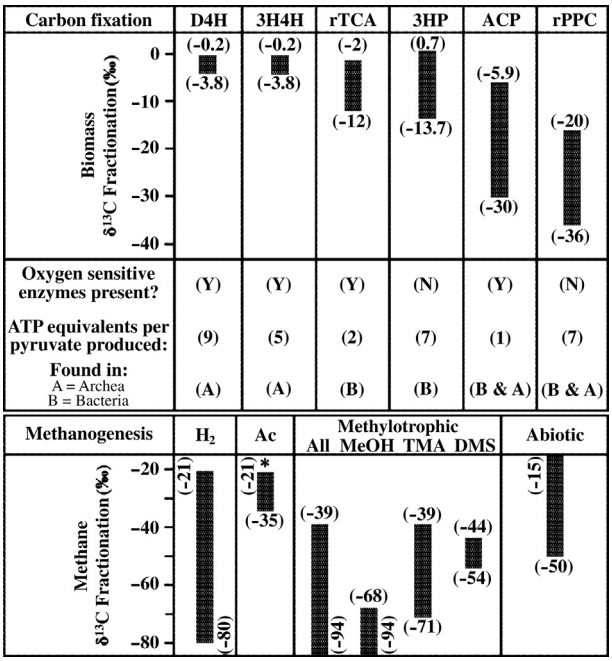

4.1. Carbon fixation

Carbon fixation is essential to sustain life on Earth. The preferential uptake of $^{12}CO_2$ and incorporation into organic matter by life results in preservation of this resulting biomass in the geologic record with carbon isotopic signatures that are isotopically lighter (i.e., with $\delta^{13}C$ values that are more negative) than the source of the CO_2.

The six known carbon fixation pathways which sustain autotrophic

growth are: the reductive pentose phosphate cycle (rPPC, a.k.a. the Calvin cycle), the reductive tricarboxylic acid cycle (rTCA, a.k.a. the reverse Krebs cycle), the 3-hydroxypropionate cycle (3HP), the dicarboxylate-4-hydroxybutyrate cycle (D4H), 3-hydroxypropionate-4-hydroxybutyrate cycle (3H4H), and the reductive acetyl-coenzyme A pathway (ACP, a.k.a. the Wood–Ljungdahl pathway) (Berg et al., 2010; Bar-Even et al., 2011). These specific carbon fixation pathways have characteristic carbon isotopic fractionations that can aid in our interpretation of the rock record (Table 2). Pure culture studies indicate the reductive acetyl-CoA pathway can impart a large fractionation (up to − 30‰ from the carbon source, Table 2). The rPPC can impart the greatest fractionation of the carbon fixation pathways (up to − 36‰, Table 2), although the fractionation of this pathway can vary based on the form of ribulose 1,5-bisphosphate carboxylase oxygenase (RuBisCO) (House et al., 2003 and references therein). The reductive pentose phosphate pathway accounts for the vast majority of carbon fixation on Earth today. It should be noted, however, that local conditions may influence the carbon isotope signal of autotrophic microorganisms. For example, microbial community $\delta^{13}C$ fractionations varied significantly (from − 3.3 to − 19.9‰) over the span of a few meters down a single hot spring outflow channel. This change was attributed to decreasing temperature and changing microbial community structure with different C-fixation pathways (Havig et al., 2011).

Phylogenetically and physiologically diverse organisms are capable of carbon fixation and the enzymes catalyzing the most mechanistically challenging steps in each pathway (i.e., RuBisCO) appeared to have evolved a single time (Berg, 2011). The generally accepted view invokes an early origin of rTCA and ACP (Wächtershäuser, 1990; Smith and Morowitz, 2004; Martin et al., 2008; Fuchs, 2011). Despite overlaps in substrates and intermediates in some of the pathways, the use of these pathways is not conserved among taxonomically related groups. For instance, the four pathways that employ acetyl-CoA and succinyl-CoA are not conserved taxonomically—rTCA and 3HP operate solely in bacterial lineages whereas the dicarboxylate-4-hydroxybutyrate and 3-hydroxypropionate-4-hydroxybutyrate cycles are used only by archaea. There is considerable overlap between the 3-hydroxypropionate and the 3-hydroxypropionate-4-hydroxybutyrate, yet the two have evolved independently (Bar-Even et al., 2011). Oxygen sensitivity, presence in both Bacteria and Archaea, and relatively high efficiency of ACP are cited as supporting circumstantial evidence for ACP as the putatively earliest evolving carbon fixation pathway (Table 2).

RuBisCO is the most abundant protein on earth for several reasons including its requirement for carbon fixation via the rPPC and its catalytic inefficiency which leads to high levels of expression to maintain growth (Ellis, 1979). Attributes of RuBisCO are often cited as evidence for an early emergence in the evolution of life including low affinity for CO_2 and competitive inhibition by O_2. Under the reducing conditions of early earth under high-CO_2 and in the absence of O_2, presumably there would not have been the selective pressure to evolve a RuBisCO enzyme able to efficiently operate under the conditions present today—high O_2 and low CO_2. RuBisCO is also plagued by slow catalytic turnover and an oxygenase side reaction (Badger and Bek, 2008). Regardless, a single explanation of the evolutionary trajectory of carbon fixation pathways has yet to be derived.

To date, the utility of interpreting the fractionation of carbon in ancient sedimentary organic matter has relied on numbers generated from organisms in pure cultures. These data have been used to constrain the magnitude of pathway-dependent carbon fractionation and infer the modes of metabolism which generated ancient sedimentary organic matter. Because systematic differences have been observed in carbon isotopic fractionation between the carbon fixation pathways, these signatures can be used as a framework to infer biogeochemical cycling of carbon in the geologic record. However, the study of ^{13}C fractionation in microbial primary producers has revealed variability in the fractionation based on organism, form of enzyme, temperature, and/or growth phase. Further complicating this is significant overlap of $\delta^{13}C$ signal produced by different carbon fixation pathways (Table 2), and potential obfuscating of these signals due to differences in C sources. These observations coupled with the complex carbon cycling that occurs in microbial ecosystems and recent discoveries of new carbon fixation pathways hinder our ability to definitively assign a metabolic origin to carbon isotope values in rock record.

While it is tantalizing to assume a metabolic pathway that is predominant today and has a similar fractionation to what is found in the rock record was the source of that fractionation, we must also remember that the genomes of extant microorganisms are an incomplete record—billions of years of evolution, extinctions, and gene loss have occurred. For instance, the more recent rock record is littered with biological macroscopic morphotypes that once dominated but are now extinct (e.g., Ediacaran fauna, Trilobites, Graptolites). In contrast, the geologic record is presumably impartial. As a result, the inference shouldn't be that a $\delta^{13}C$ fractionation of − 25‰ found at 3.5 Ga was produced by the pentose phosphate cycle, but rather when we observe such a fractionation, our best available model to use is a modern analog that exhibits a similar fractionation. Still, 3.5 billion years of evolutionary (and geochemical/geologic) pressure has been exerted, and it is not only possible but likely that metabolic pathways long ago lost existed which could produce an equivalent fractionation to those known today. Similarly, as processes evolved to become more efficient or energetically favorable, a more consistent fractionation might have resulted.

4.2. Photosynthesis

The link between the redox history of the Earth's surface and photosynthesis is tied to the fundamental transfer of electrons through C-fixation as CO_2 is converted into CH_2O. Historically, the most attention has been given to oxygenic photosynthesis:

$$CO_2 + H_2O + h\nu \Rightarrow CH_2O + O_2,$$

whereby the powerful oxidant O_2 is released on the Earth's surface and a fraction of the organic material has the potential to be buried and locked away, effectively removing 4 electrons from the Earth surface for every C buried, and leaving a molecule of O_2 (Fig. 5). However, alternatives to oxygenic photosynthesis have been found in modern systems, termed anoxygenic photosynthesis, and these forms may have predated oxygenic photosynthesis by as much as 1.2 Ga (Battistuzzi et al., 2004; Olson, 2006). Anoxygenic photosynthesis can be carried out using reduced sulfur compounds such as H_2S and S^0 (Table 1), as well as with hydrogen:

$$CO_2 + 2\,H_2 + h\nu \Rightarrow CH_2O + H_2O,$$

and with iron:

$$4\,Fe^{2+} + CO_2 + 11\,H_2O + h\nu \Rightarrow CH_2O + 4\,Fe(OH)_3 + 8H^+$$

All of these pathways serve as a mechanism for burying electrons as organic material and thus contributing to the net oxidation of the earth's surface, but not necessarily accumulation of oxygen.

In some extant environments such as photic zones where oxygen and sulfide co-exist, the ecological niches of anoxygenic phototrophs and Cyanobacteria can overlap (Klatt et al., 2011, 2013). For instance, in some stratified lakes, the oxic/anoxic interface is shallow and supports dense layers of anoxygenic phototrophs. These conditions mimic those thought to be present in areas of the Proterozoic oceans, especially along continental shelf margins. In these systems today, anoxygenic photosynthesis can be the main source of primary production (Van Gemenden and Mas, 1995).

In addition to the photoautotrophic means for fixing carbon described above, there are also photoheterotrophic pathways that can use light energy to power the addition of CO_2 to organic molecules, such as:

$$C_3H_4O_3\,(\text{pyruvate}) + CO_2 + H + h\nu \Rightarrow C_4H_5O_5\,(\text{malate}).$$

In this case, the CO_2 used can come from heterotrophic breakdown of organic material (as opposed to the DIC pool), so there is no effect on the net burial of electrons. However, if there is enough cycling of organic material by photoheterotrophs to enrich the resulting biomass through selective uptake of $^{12}CO_2$, driving the overall organic carbon $\delta^{13}C$ signal more negative, then photoheterotrophy may play a role in altering the organic carbon $\delta^{13}C$ signals preserved in the rock record. Laboratory pure culture experiments would help to shed light on this speculative idea.

4.3. Methanogenesis

All methanogenesis pathways (only known for archaea) share the use of the nickel enzyme methyl-coenzyme M reductase (encoded by *mcr*) to catalyze the conversion of substrates and formation of methane (Jaun and Thauer, 2007). Methanogenesis has long been postulated as one of the oldest energy yielding metabolic pathways used by life (e.g., Walker, 1977; Wächtershäuser, 1990) and methanogens have been indicated to be the ancestors of all archaea (Borrel et al., 2016). Supporting the idea of an early evolution and subsequent loss of methanogenesis is the recent discovery of *mcr* gene sequences in Bathyarchaeota, providing the first evidence of methanogens outside of the Euryarchaeota (Evans et al., 2015; Lever, 2016). The microbially mediated generation of methane (CH_4) is categorized by three known pathways: hydrogenotrophic, acetoclastic, and methylotrophic. Hydrogenotrophic methanogenesis involves an eight step process to catalyze the reduction of CO_2 into CH_4 (Costa and Leigh, 2014), summarized by the reaction $4\ H_2 + CO_2 => CH_4 + 2\ H_2O$. Acetoclastic methanogenesis uses the same final three steps as hydrogenotrophic methanogenesis, with the amendment being the uptake and conversion of acetate to acetyl-CoA from which the methyl group enters the methanogenesis machinery following its transfer onto the carrier tetrahydromethanopterin (H_4MPT), entering as methyl-H_4MPT (Costa and Leigh, 2014). The overall chemical reaction for this reaction is $CH_3COOH => CH_4 + CO_2$. Methylotrophic methanogenesis uses the equivalent of the last two steps of hydrogenotrophic methanogenesis, converting methylated substrates into methyl-S-CoM (methyl-sulfhydryl-coenzyme M) (Costa and Leigh, 2014). Examples of reactions carried out by methylotrophic methanogens include use of methanol ($4\ CH_3OH => 3\ CH_4 + CO_2 + 2\ H_2O$), formate ($4\ CHOOH => CH_4 + 3\ CO_2 + 2\ H_2O$), trimethyl amine ($4\ (CH_3)_3N + 6\ H_2O => 9\ CH_4 + 3\ CO_2 + 4\ NH_3$), and dimethylsulfide ($2\ (CH_3)_2S + 3\ H_2O => 3\ CH_4 + CO_2 + H_2S$).

Microbially mediated methanogenesis imparts a negative signal upon the produced methane due to preferential selection of ^{12}C. Typically, CH_4 with $\delta^{13}C$ values more negative than −50‰ are assumed to be biogenic, while less negative values are assumed to be derived from abiotic thermogenic breakdown of organic matter, but the signals can overlap (Whiticar, 1999). The final $\delta^{13}C$ value of CH_4 is dependent upon the $\delta^{13}C$ value of the C source substrate, as well as other factors such as methanotrophy (biologically-mediated oxidation of CH_4) and diffusion effects. Measured fractionation factors for CH_4 generated in pure culture experiments suggest some ability to associate values with specific pathways, though there is significant overlap in fractionation factors for different pathways as well as with fractionations determined from abiotic experiments (Table 2). This overlap is further complicated by effects from environmental conditions such as temperature and pressure (e.g., Takai et al., 2008) and substrate concentration (e.g., Londry et al., 2008; Goevert and Conrad, 2009), as well as differing $\delta^{13}C$ values of C substrate. However, all forms of biogenic methanogenesis instill a $\delta^{13}C$ fractionation resulting in CH_4 more negative than its C source, and methanotrophic organisms (which gain energy from oxidizing CH_4, and convert CH_4 into biomass) consistently have biomass $\delta^{13}C$ values reflecting that (−29 to −85‰, Schidlowski, 2001).

4.4. Fermentation

Prior to the presence of free oxygen, anaerobic heterotrophic breakdown of organic matter was the primary driver of biological biomass degradation for cycling organic carbon back into the carbon cycle. Larger organic molecules are broken down by specific enzymes: polysaccharides (such as cellulose, pectin, and starch) can be hydrolyzed to glucose (via cellulases, pectinases, and amylases); lipids can be converted into long-chain fatty acids by the action of lipases; and proteins can be hydrolyzed to amino acids via proteases (with amino acids further broken down into fatty acids and ammonia). Fatty acids can be broken down anaerobically, such as by H_2-producing acetogenic bacteria via different reactions depending on whether there is an odd or even number of carbons in the fatty acid. As examples, 4-carbon butanoic acid is broken down into acetic acid and hydrogen following the reaction: $C_4H_8O_2 + 2\ H_2O => 2\ CH_3COOH + 2\ H_2$, and 5-carbon pentanoic acid into propanoic acid, acetic acid, and hydrogen following the reaction: $C_5H_{10}O_2 + 2\ H_2O => C_3H_6O_2 + C_2H_4O_2 + 2\ H_2$. Glucose can be broken down anaerobically through processes such as fermentation, producing CO_2 and ethanol (e.g., $C_6H_{12}O_6 => 2\ CH_3COOH + 2\ CO_2$); and mixed acid fermentation which can produce a wide array of end products such as lactic acid, acetic acid, formate, ethanol, CO_2, and H_2 (e.g., $C_6H_{12}O_6 + 4\ H_2O => 2\ CH_3COOH + 2\ CO_2 + 4\ H_2 + 2\ H_2O$).

Currently, the effects of fermentation on the carbon isotopic signal in the rock record are poorly constrained, but recent work on fractionation imparted through fermentation in pure culture and environmental studies provide some insight. Pure culture experiments have demonstrated that fermentation of glucose can impart different fractionations on the $\delta^{13}C$ values of end products, including ethanol (−6.9 to −13.0‰), acetic acid (+4.0 to +8.0‰), and lactose (−1.6 to −6.1‰) as well as biomass (−1.4 to −5.9‰) (Penning and Conrad, 2006). Furthermore, fractionation of $\delta^{13}C$ values of acetic acid generated from the fermentation of polysaccharides (from cellobiose: +4.5 to +8.8‰, Penning and Conrad, 2006; from pectin: +5.5‰, from xylan: +2.1‰, from starch: −2.6‰, Botsch and Conrad, 2011) as well as propionic acid generated from the fermentation of polysaccharides (from pectin: −4.0‰, from xylan: −7.6‰, from starch: −7.9‰, Penning and Conrad, 2006) suggest the potential for a complex carbon isotope effect. Comparison of analyses in multiple environmental settings show acetic acid $\delta^{13}C$ values are generally enriched by +1.5 to +16.3‰ compared to the total organic carbon, while incubation experiments with environmental samples show a much greater range, with acetic acid enriched by −6.4 to +26.7‰ (Heuer et al., 2006). Anaerobic incubations of sediments and soils in the presence of CH_3F (which inhibits the activity of acetoclastic methanogens) showed acetic acid $\delta^{13}C$ values fell between −10 to +10‰ of the $\delta^{13}C$ values of the total organic carbon (Conrad et al., 2014). These results suggest that acetic acid consuming metabolisms favor isotopically lighter acetic acid. Fermenters grown exclusively on glucose or cellobiose had biomass $\delta^{13}C$ values that indicated preferential incorporation of isotopically light carbon ($\delta^{13}C$ enrichments of −1.4 to −5.9‰ and −0.1 to −1.7‰, respectively, Penning and Conrad, 2006), though results of pure culture experiments with SROs grown on acetic acid showed biomass $\delta^{13}C$ enrichments that ranged from −7.4 to +8.6‰ (Londry and Des Marais, 2003; Goevert and Conrad, 2008), indicating more study is needed. From these studies, we tentatively postulate that accumulation of fermenter biomass at the expense of organic carbon in sediments would tend to result in organic carbon deposits composed of significant fermenter biomass more negative, while biomass generated from the products of fermentation will depend on the fermentation product consumed.

5. Electron transfer and geologic processes

A simplified conceptual cartoon to illustrate the movement of

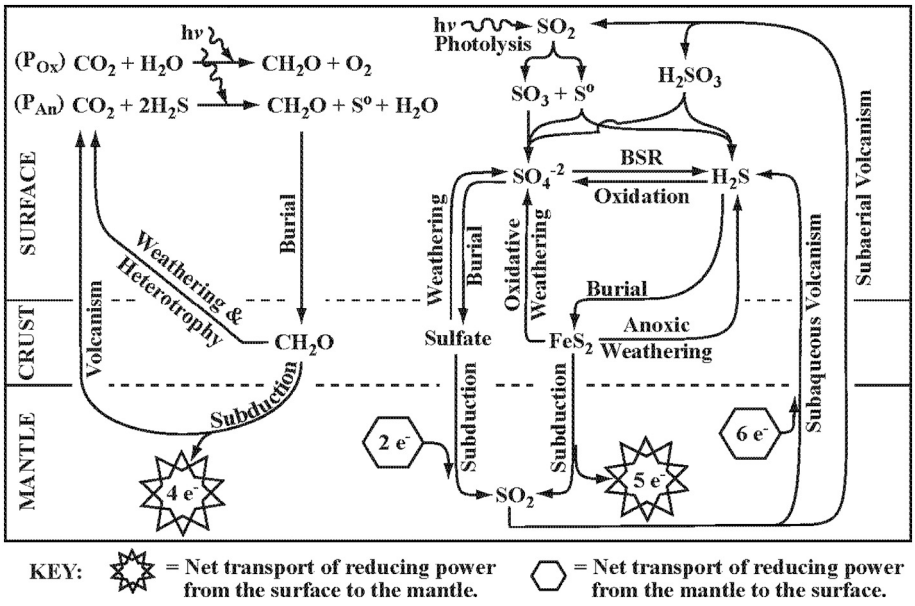

Fig. 4. Conceptual cartoon illustrating the movement of reducing power between the surface, crust, and mantle through the carbon and sulfur cycles.

electrons (e^-) through the surface system of earth and means for transporting reducing power between the mantle and surface is presented (Fig. 4). For the carbon system, volcanism releases CO_2 into the atmosphere, which can be reduced to organic carbon (represented by CH_2O) through either oxygenic photosynthesis (utilizing photons to break the H—O bonds in water, and producing O_2) or anoxygenic photosynthesis (represented by the photolytic breakdown of H_2S, generating S^0). Through incomplete reoxidation of the produced organic carbon and burial of that reduced material, the reducing equivalent of 4 e^-s are removed from the surface. If that organic material is then subducted and delivered into the mantle, the CH_2O is oxidized to CO_2, and the 4 e^-s are effectively removed from the surface. In the sulfur system, sulfur can be delivered either as the more oxidized SO_2 through subaerial volcanism, or as H_2S (through the reaction of H_2S with H_2, Table 1) through subaqueous volcanism. In the surface system, SO_2 can be combined with H_2O to produce sulfite, or it can undergo photolysis (the process that can impart a MIF signal) to generate SO_3 or S^0. The SO_3 can then react with H_2O to generate SO_4^{2-}, and disproportionation can convert SO_3^{2-} or S^0 into SO_4^{2-} and H_2S (Table 1). Biological sulfate reduction and oxidation can then intermix these pools of sulfur, and sulfide can be sequestered at pyrite or SO_4^{2-} as sulfate minerals. Upon subduction, all sulfate and sulfide minerals are converted into SO_2 in the mantle, and pyrite will deliver 5 e^-s to the mantle upon conversion to SO_2 while sulfate will consume 2 e^-s. When the SO_2 is converted to H_2S during subaqueous volcanism, there is a delivery of 6 e^-s to the surface from the mantle. Thus, burial and/or subduction of

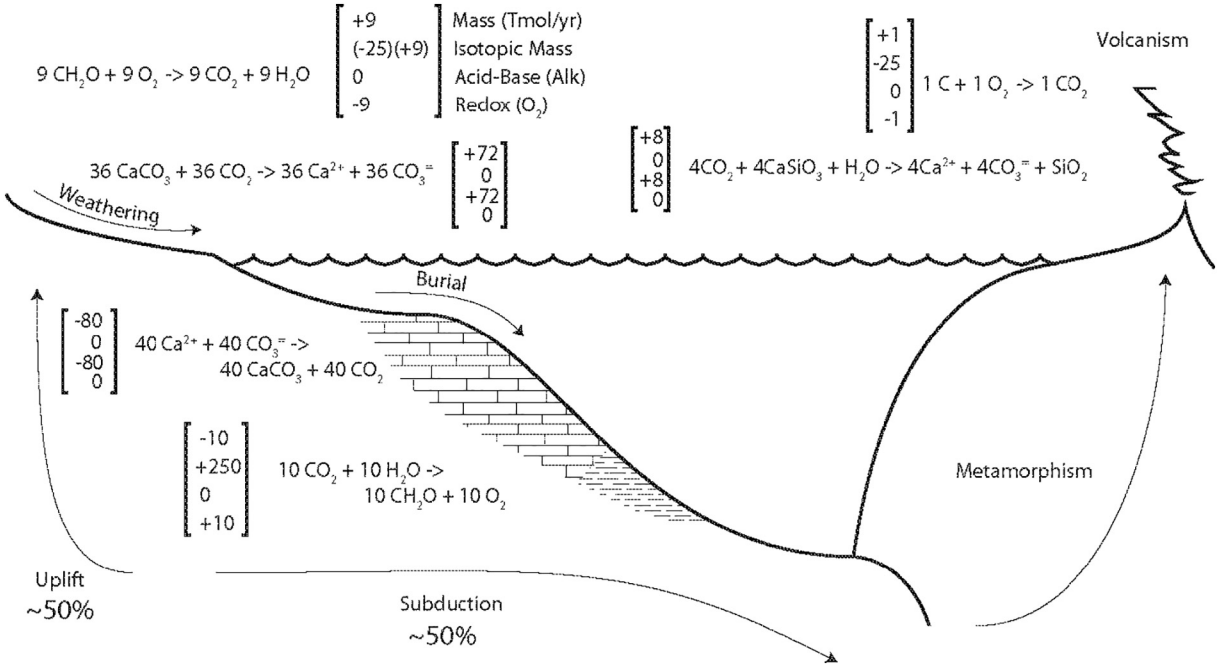

Fig. 5. Cartoon of the geologic carbon cycle. Arrows and reactions indicate transformations of carbon. Coefficients of reactions are in Tmol/yr. Each reaction can be assigned a vector quantity which indicates the impact of the transformation on mass, isotopic mass, acid-base (alkalinity), and redox (O_2) from the perspective of the ocean-atmosphere system. For instance the oxidation of organic carbon contributes 9 Tmol·yr of carbon to the ocean-atmosphere system, and $-25 * 10 = -250$ Tmol ‰ of carbon isotopic mass units. The reaction has no impact on alkalinity, and 10 Tmol/yr of O_2 are consumed by it.

pyrite sourced from SO_2 results in removal of 5 e^-s from the surface, while burial of sulfate results in the addition of 2 e^-s. A conceptual model representing the carbon cycle demonstrates the influences of the carbon transformations on mass, isotopic mass, alkalinity, and redox for the ocean-atmosphere system (Fig. 5).

6. Rock record and theoretical contextual information

Multiple lines of direct and indirect contextual information relating to the redox evolution of the Earth's surface are available from the literature to elucidate the setting for and effects of the evolving earth and developing biosphere on the sulfur and carbon isotope systems. These include geologic and geochemical analyses and interpretation of the rock record, including mantle cooling; crustal thickness, cycling, and formation; and redox-related evidence. This section briefly describes and summarizes the current knowledge of the contextual components which are shown in Fig. 6.

6.1. Apparent percent melt and preserved crustal thickness

Estimates for rates of stable continental crust growth have been undertaken based on geochemical analyses. Rates of continental landmass accumulation are based on element composition analyses of crustal material (Taylor and McLennan, 1995; Fig. 6B, darker grey line) or on Th-U-Nd systematics of the mantle (Collerson and Kamber, 1999; Fig. 6B, lighter grey line). A higher temperature mantle will produce a greater percentage of melt, while a cooler mantle would allow for preservation of generated crustal material. Apparent percent melt (APM) decreasing with time is consistent with secular cooling of the mantle as heat was lost from surface cooling coupled to a decline in radiogenic decay heat production (Keller and Schoene, 2012). A high APM during the Eoarchean (4.0 to 3.6 Ga) (Fig. 6A) is consistent with the presence and recycling of Hadean crust through delamination until circa 3.6 Ga. This also suggests slow recycling and a long residence time (~750 Ma) for the initial Hadean crust that crystalized from the magma ocean that followed the moon-forming impact (Roth et al., 2014). The Eoarchean and Paleoarchean (3.6 to 3.2 Ga) was the time of the formation of the oldest cratons (e.g., Kaapvaal in South Africa, Wyoming and Slave in North America, Pilbara in Australia, Dwarhar in India). Preserved crustal thickness (PCT) decreasing from the Eoarchean to the Paleoarchean would be consistent with a transition from a delamination-dominant to a subduction-dominant regime, with older Hadean crustal material being replaced with thinner spreading-derived oceanic crust, and stabilization of small, thicker cratons (Fig. 6A). Increasing PCT through the Paleoarchean, Mesoarchean (3.2 to 2.8 Ga), and Neoarchean (2.8 to 2.5 Ga) are consistent with increasing continental

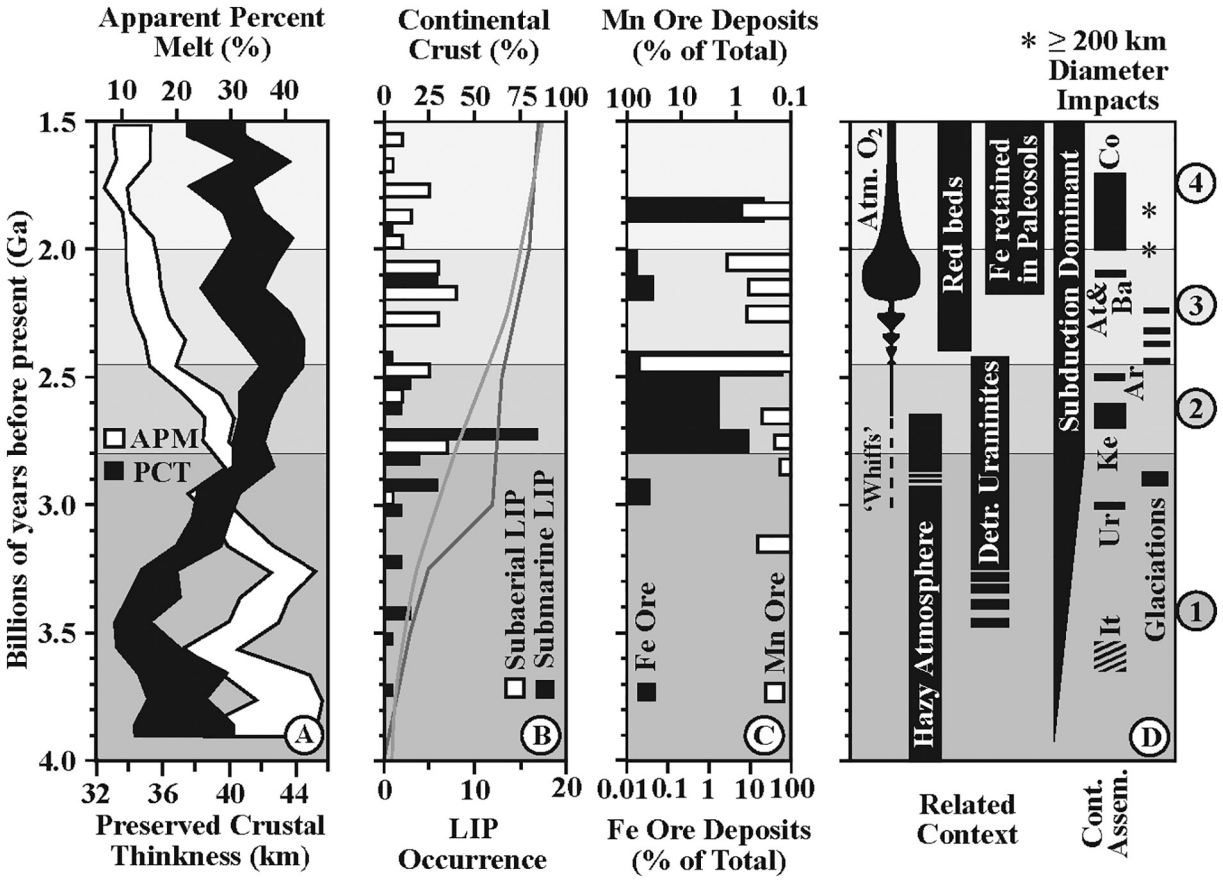

Fig. 6. Rock record data related to sulfur chemistry and the history of oxidation of the earth's surface. A) Apparent percent melt (APM) and preserved crustal thickness (PCT) adapted from modeling by Keller and Schoene (2012) of composite igneous rock record data. B) Percent of continental crust formed according to Taylor and McLennan (1995) (darker grey line) and Collerson and Kamber (1999) (lighter grey line) and occurrence of subaqueous (black) and subaerial (white) large igneous province (LIP) formation through time, tallied into 0.10 Ga bins. LIP data from Kump and Barley (2007). C) Percent of estimated global iron ore deposits (as banded iron formations, or BIFs) and percent of estimated global Mn ore deposits, tallied into 0.10 Ga bins. Iron ore data (black bars) from Bekker et al. (2010), Mn ore data (white bars) from Maynard (2010) and Gumsley et al. (2017). Note logarithmic scales. D) Other rock record data related to the oxygenation of the earth's surface. Oxygenation evidence from Anbar et al. (2007); Wille et al. (2007); Holland (2009); Frei et al. (2009); Crowe et al. (2014); and Gumsley et al. (2017). Paleosol information from Rye and Holland (1998). Red beds and detrital grain information from Catling and Claire (2005). Detrital uraninite information from Johnson et al. (2014). Support for a hazy atmosphere during the Archean from Wolf and Toon (2010). Initiation of assembly of Archean cratons into stable continents (It = putative first continent 'Itsaqia', Ur = 'Ur', Ke = 'Kenorland', Ar = 'Arctica', At = 'Atlantica', Ba = 'Baltica', Co = first supercontinent 'Columbia') from Rogers and Santosh (2003); Lubnina and Slabunov (2011); Roberts (2013); Condie (2014); Nutman et al. (2015); and Gumsley et al. (2017). Glaciation timing from Young et al. (1998); Rasmussen et al. (2013); and Gumsley et al. (2017).

mass, and stabilization of PCT through the Paleoproterozoic (2.5 to 1.6 Ga) suggests a relative steady state for continental crust production and destruction. Alternatively, an interpretation of Rb/Sr ratios in juvenile crust going back to the Hadean as an indicator for differentiation suggests new crust formed prior to ~3 Ga was predominantly mafic, suggesting subduction was not a major driver of differentiation of crustal material until this time (Dhuime et al., 2015).

6.2. Tectonic setting and continent formation

Continental formation heralds the amalgamation of cratons to form stable continents—platforms capable of maintaining sedimentary deposits for long periods of time and allowing protection of substantial amounts of materials from crustal recycling. The first continent ('Itsaqia') is posited to have begun assembly circa 3.66 Ga, suggesting the initiation of subduction and a Wilson Cycle as early as 3.9 Ga (Nutman et al., 2015). Evidence for the assembly of a large continent include is evident around 2.7 to 2.6 Ga ('Kenorland') and the first supercontinent around 2.0 to 1.7 Ga ('Columbia') (Roberts, 2013; Condie, 2014). Assembly of smaller continental masses include 'Arctica' starting ~2.5 Ga, and 'Atlantica' and 'Baltica' starting ~2.1 Ga (Rogers and Santosh, 2003; Condie, 2014). The beginning of the assembly of smaller cratons into larger continental land masses serves as an indicator of modern style plate tectonics (Fig. 6D), though some have used geochemical modeling of formation of tonalite-trondhjemite-granodiorite cores of Archean cratons to suggest subduction may not have initiated until 3.5 Ga (Johnson et al., 2017). Others have argued based on shifts in bulk MgO compositions of Archean upper continental crust to suggest an onset of subduction as late as 3.0 Ga (Tang et al., 2016). The progressive stabilization of cratons into continents is consistent with the beginning of a secular increase in preserved crustal thickness starting around 3.5 Ga (Keller and Schoene, 2012), and supports subductive overturn of crustal material had begun by that time.

6.3. Large igneous provinces

LIPs are defined as large (areal extent > 0.1 M km^2, volume > 0.1 M km^3) intraplate volcanic units characterized by the majority of material (> 75%) emplaced over short pulses (~1 to 5 Ma) (Bryan and Ernst, 2008). The first evidence of a subaerial large igneous province is found on the Kaapvaal craton dated at 2.94 Ga, and marks the beginning of a transition from predominantly submarine large igneous province formation to subaerial, occurring between 2.8 and 2.5 Ga (Kump and Barley, 2007) (Fig. 6B). The eruption of subaerial LIPs would have provided a large source of SO_2 into the atmosphere. LIP formation is linked to the rapid accumulation of continental crust from ~3.0 to 2.0 Ga, with an estimated 70% of modern continental landmass produced during this time (Fig. 6B).

6.4. Iron and manganese deposits

Banded iron formations (BIFs) are iron ores defined as layered, bedded, or laminated stratigraphic units composed of ≥15% weight iron that often contain quartz, chert, or carbonate interlayers (James, 1954; Gross, 1980). Peak BIF formation, producing over 95% of the estimated global iron ore, occurred from ~3.2 to 1.8 Ga, with the earliest BIFs found in the Isua terrain of Greenland. For in-depth discussion on BIFs, see Isley and Abbott (1999) and Bekker et al. (2010). Approximately 75% of iron ore was deposited from 2.8 to 2.4 Ga, with a second pulse from 1.9 to 1.8 Ga (Fig. 6C). The provenance of BIFs has been linked to abiotic oxidation by oxygen produced via oxygenic photosynthesis (Swanner et al., 2015), or to direct oxidation of Fe^{2+} to Fe(III) via anoxygenic photosynthesis (Bekker et al., 2010). Modern analogs have been described where anoxygenic photosynthesis is directly linked to Fe^{2+} oxidation (Crowe et al., 2008; Walter, 2011; Walter et al., 2014). Thus, the presence of BIFs may serve as an indicator of anoxygenic photosynthetic activity in Archean and Proterozoic oceans, with the source of Fe^{2+} for peak BIF formation linked to the eruption of large igneous provinces (Isley and Abbott, 1999).

Manganese ore deposits are thought to primarily form under two regimes, either as sedimentary deposits of manganous carbonates (e.g., rhodochrosite - $MnCO_3$; kutnahorite - $MnCa(CO_3)_2$) at redox transition zones (e.g., oxic-euxinic boundary in basins) which make up over 93% of total ore reserves, or to a lesser extent as volcanic rock hosted (mostly as the manganese silicate braunite) deposits which make up approximately 6% of reserves (Maynard, 2010). Of the total known global manganese ore reserves, over 63% were deposited during the Paleoproterozoic (Fig. 6C). The timing of the deposition of the largest known manganous ore deposit (the Hotazel Formation of the Postmasburg Group in South Africa, alone making up 60% of known global manganese ore reserves) occurred between 2.42 and 2.39 Ga immediately after the first of four Paleoproterozoic glaciations which has been suggested to be a "Snowball Earth" event (Gumsley et al., 2017). A putative link between manganese carbonate precipitation in the water column and biologic maintenance of high manganese concentration at the oxic-euxinic boundary of a redox stratified lake provides a potential mechanism for precipitation of manganese ore (Havig et al., 2015), and is consistent with the presence of oxygen oases into the Archean (Olson et al., 2013) and possible precipitation of associated manganous carbonates prior to and following the GOE. An alternative interpretation by Johnson et al. (2013) invokes the onset of a Mn-oxidizing photosystem (a precursor to photosystem II) as the source of precipitated Mn ores at 2.415 Ga, an idea that is challenged by evidence for free oxygen produced apparently by pelagic cyanobacteria using photosystem II during the Archean (e.g., Anbar et al., 2007); isotopically light 2.7 Ga organic matter (Schidlowski et al., 1983); Archean metal and isotope studies (e.g., Crowe et al., 2014, Reinhard et al., 2013), and molybdenum isotopes suggesting the presence of manganese oxides at 2.95 Ga (Planavsky et al., 2014).

6.5. Early hazy atmosphere

The composition and oxidation state of the atmosphere is indicated in many aspects of the rock record (Holland, 1994). An early hazy atmosphere predicted for the Archean (Fig. 6D) was first proposed by Lovelock (1988), where he described observing the Earth from space as such: "The view would have been of a brownish-red hazy planet…" This hazy atmosphere required a reduced atmosphere replete in methane, which provided effective protection from UV radiation (Domagal-Goldman et al., 2008; Haqq-Misra et al., 2008; Wolf and Toon, 2010). Haze is generated via the production of methyl radicals ($\cdot CH_3$) through photolysis of CH_4, or from the reaction of CH_4 with the $\cdot OH$ radical (produced via photolysis of H_2O). In low O_2 atmospheres, methyl radicals react to form C_2H_6. Photolysis of C_2H_6 can produce C_2H_4 and C_2H_2, and reaction of C_2H_6 with the $\cdot OH$ radical can lead to three and four-carbon molecules. All of these organic molecules produce an extensive organic haze (Haqq-Misra et al., 2008). The presence of an organic haze would have blocked UV radiation while potentially remaining relatively transparent in mid-wavelengths, minimizing cooling effects (Wolf and Toon, 2010). A UV-opaque organic haze would have suppressed the mass independent fractionation of S in the atmosphere, which is thought to predominantly occur due to UV radiation between 190 and 220 nm (Farquhar et al., 2001) and 250 to 350 nm (Whitehill et al., 2013).

6.6. Detrital uraninites

Uraninite (UO_2) is a redox-sensitive mineral that forms as primary constituents of granites and pegmatites as well as in medium to high temperature hydrothermal veins. Uraninite readily oxidizes in the presence of oxygen, but in the absence of O_2 it will weather out of rocks and be transported to low-energy sedimentary environments to form

placer deposits. The absence of detrital uraninite grains in deltaic deposits (suggesting transport over 100s of kilometers) indicates atmospheric oxygen concentrations above 3.2×10^{-5} atm (Johnson et al., 2014). Thus, the presence or absence of detrital uraninites serves as a useful indicator for the presence of low levels of free oxygen in the atmosphere, and their presence until 2.42 Ga serves as a constraint on the presence of sustained free oxygen in the atmosphere (Fig. 6D).

6.7. Occurrence of red beds

Red beds derive their hue from the presence of oxidized iron, and thus serve as an indicator of the presence of atmospheric oxygen. Red beds carry two definitions. The first, given by Hatch and Rastall (1965) and most widely used, define red beds in a strict sense as arenaceous to argillaceous (sand-sized to clay-sized) clastic sedimentary rocks deriving a red hue from ferric oxide coating of individual grains, with > 60% of a succession red. A second less rigorous definition was proposed by Van Houten (1973) which defined red beds as detrital sedimentary rocks with red ferric oxides occurring as grain coatings, pore fillings, or dispersed within matrix clays. Currently there is no set atmospheric O_2 concentration associated with the formation of red beds, limiting the utility of red beds to a yes/no indicator of free atmospheric oxygen, first observed circa 2.4 Ga (Catling and Claire, 2005; Fig. 6D).

6.8. Iron retention in paleosols

Paleosols, loosely defined as a soil that formed on a landscape or in an environment of the past (Neuendorf, 2005), provide another potential indicator of atmospheric composition. Soils represent an interface between rock and atmosphere during breakdown and weathering of a terrestrial surface. Prior to free O_2 in the atmosphere, weathering of minerals liberated Fe^{2+}, which would have been mobile similar to Ca^{2+} and Mg^{2+}. In contrast, in the presence of atmospheric O_2, Fe^{2+} would be oxidized to insoluble Fe(III), precipitated as iron oxides, and retained in the developing soil. Rye and Holland (1998) conducted a review of Archean and Proterozoic paleosols, using a strict set of criteria for classifying units as paleosols: the unit must have developed on a homogenous parent rock; it must have been preserved in place; it must exhibit changes in mineralogy, texture, and chemical composition from the parent rock to the top of the soil consistent with soil formation; and there must be identifiable soft-sediment deformation at the contact between the proposed soil and the overlying unit. Based on this criteria, they identified 15 definite paleosols (met all criteria) and 13 likely paleosols (met 4 of five criteria). In paleosols with ages > 2.44 Ga, there is evidence for iron mobilization and loss as soluble Fe^{2+} during weathering consistent with very low atmospheric O_2 concentrations. In younger paleosols (formed after 2.20 Ga) there is strong evidence that iron was retained during weathering and red beds are common in units that overly the paleosols, consistent with atmospheric O_2 concentrations > 0.03 atm (Rye and Holland, 1998), and this is the time that we assume to represent a significant increase in the concentration of free O_2 in the atmosphere (Fig. 6D). In three paleosols that fall between those ages, the evidence for retention or loss of iron is ambiguous, but the presence of red beds above the paleosols suggest there were intermediate or fluctuating atmospheric O_2 concentrations during that time. More recent modeling efforts to estimate the pO_2 for the Paleoproterozoic based on Fe profiles in five paleosols that range in age from 2.46 to 1.85 Ga was done, incorporating estimates of weathering parameters such as porewater pH, CO_2 partial pressure, water flow, temperature, and diffusion of O_2 into soil (Kanzaki and Murakami, 2016). The results of this work indicate that just prior to the GOE (at 2.46 Ga), O_2 was equal to or less than $\sim 10^{-5.4}$ atm, whereas afterwards it ranged from $\sim 10^{-5}$ to $10^{-2.5}$ (2.15 Ga paleosol) or from $\sim 10^{-5.2}$ to $10^{-1.7}$ atm (2.08 Ga paleosol). It should be noted that patterns of iron loss and retention of redox-sensitive minerals in Mesoproterozoic paleosols (~1.1 Ga) have been interpreted as a reduced role of O_2 in weathering, implying a lower atmospheric O_2 concentration for that time period (Mitchell and Sheldon, 2016), and indicating decreased atmospheric O_2 concentrations following the Paleoproterozoic.

6.9. Glaciation events

Glacial periods on the early earth signal putative changes in atmospheric composition with the loss of greenhouse gases decreasing the atmosphere's ability to trap heat on the Earth's surface, resulting in a cooling of the surface. Evidence for the first low latitude glaciation event at ~2.9 Ga (Fig. 6D) is found on the Kaapvaal Craton as diamictites (unsorted to poorly sorted terrigenous sediments) of putative glacial origin within the Mozaan Group sediments of the Pongola Supergroup (Young et al., 1998). The second low latitude glacial event is a series of four glaciations that occurred from ~2.42 to 2.15 Ga (Bekker and Holland, 2012; Hoffman, 2013; Gumsley et al., 2017).

7. Interpretation of sulfur isotope data

Using a mass balance modeling approach, we can interpret some of the trends observed in the $\delta^{34}S$ values in the rock record. The first order trends that we observe in the data in periods 2, 3, and 4 (2.8 Ga to 1.5 Ga) are: an increase in the $\delta^{34}S$ of sulfate minerals from approximately +10‰ to +40‰, a roughly parallel increase in the upper envelope of $\delta^{34}S$ values of sulfide minerals, and a decline of the lower envelope of $\delta^{34}S$ values of sulfide minerals from about 0‰ to −40‰ followed by an increase from −40‰ back to approximately 0‰.

We interpret these trends using a simple isotope mass balance model for sulfur. At steady state, the sulfur isotopic composition of the ocean (which is also the $\delta^{34}S$ value of sulfate minerals precipitating from it) is given by:

$$\delta^{34}S_{sulfate} = \delta^{34}S_{input} + f_{py} * \Delta_S$$

where f_{py} is the fraction of the total sulfur output fluxes from the ocean that occur as pyrite, and Δ_S is the fractionation imparted to sulfide minerals during sulfate reduction and subsequent precipitation relative to ambient sulfate in seawater and pore water. This expression is analogous to the expression relating the carbon isotopic composition of the ocean to the burial fraction of organic carbon and can be derived in the same way. Over the timescale of interest, the input of sulfur is assumed to have been dominated by mantle input with an isotopic composition of approximately zero, though some have suggested significant subduction of sulfides (e.g., Reinhard et al., 2013) potentially influencing the sulfur isotope signal of sedimentary sulfides in the upper crust. We can obtain estimates for the fraction of sulfide burial by estimating the values of Δ from the difference between the $\delta^{34}S$ of sulfate and sulfide minerals and assuming that the mantle input to the surficial systems has not deviated substantially from near 0‰. Fig. 7 shows the distribution of the pyrite and organic carbon burial fractions obtained by randomly drawing (statistics table presented in SOM) sulfide and sulfur $\delta^{34}S$ from each bin and calculating f_{py}.

For most of the time interval examined, the majority of calculated f_{py} values (the peaks in the kernel density diagrams, Fig. 7) have a value near 1. This observation indicates that the majority of time sulfur was burined in reduced form. Specifically, during Period 1 (4.0 to 2.8 Ga) the median values of sulfide minerals is 0.5‰, which is sufficiently near the value of mantle to suggest that pyrite was the predominant species of sulfur being removed from the ocean. That the fractionation was likely close to 5‰, as indicated by the median isotopic value of sulfate minerals which is 4.67‰. Locally increased availability of sulfate might account for sulfide minerals with negative $\delta^{34}S$ values which occur from 3.5 to 3.2 Ga. Mechanisms for increased fractionation might include “oxygen oases” (Olson et al., 2013), “whiffs of O_2” (Anbar et al., 2007), or the production of sulfate via anoxygenic photosynthesis (Thompson

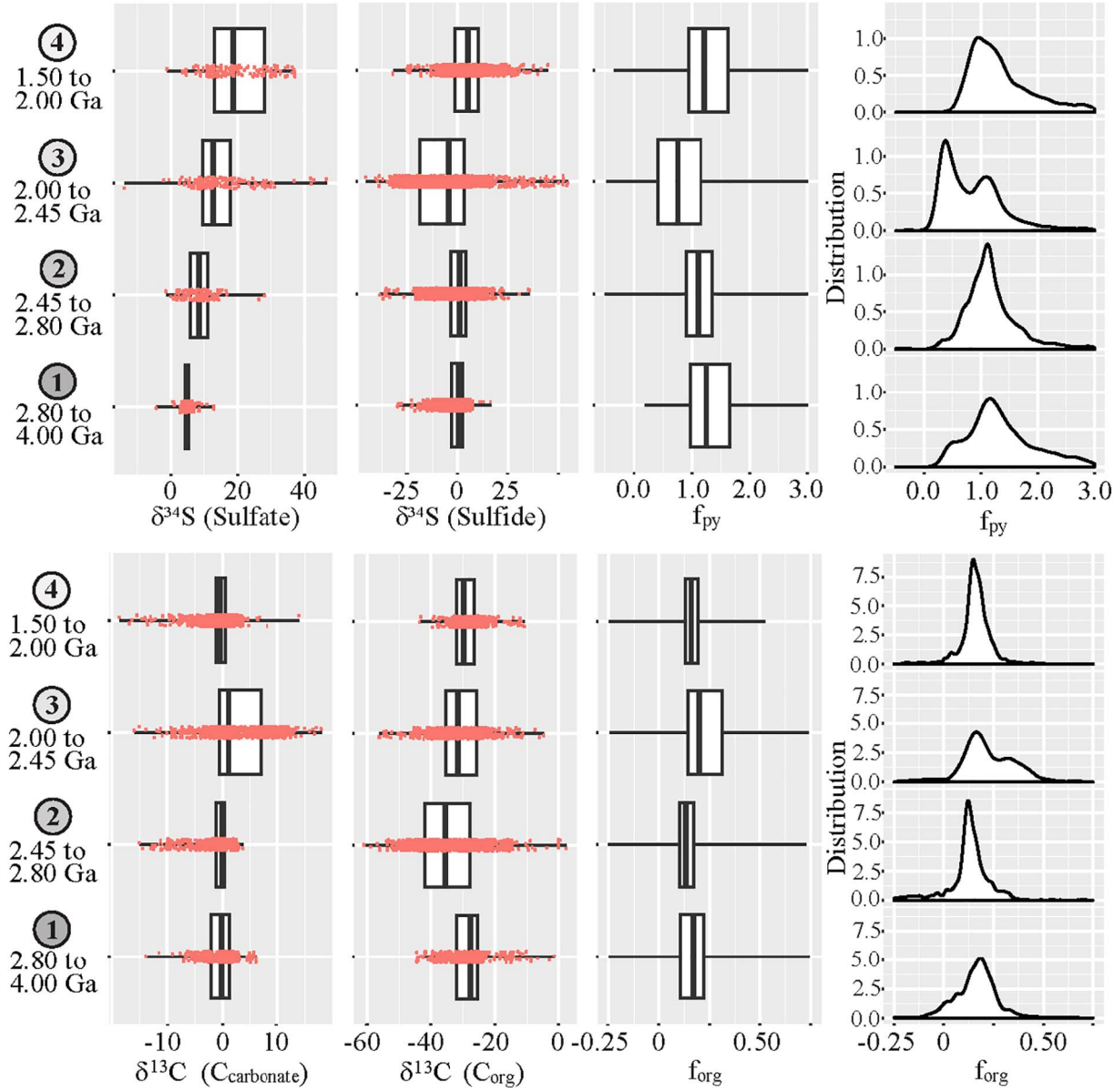

Fig. 7. Sulfur and carbon isotopic composition and calculated fraction of burial (f_{py} and f_{org}). Data binned according to time periods described in text. Each bin was randomly subsampled 1000 times and f_{py} or f_{org} calculated on the pairs of points (shown in red) drawn from the reduced and oxidized species. The resulting calculated distribution for f_{py} and f_{org} is plotted in the right two columns, once as a box plot and once as a kernel density plot.

et al., 1990) and/or disproportionation (Janssen et al., 1996; Canfield, 2001) prior to biological sulfate reduction (BSR). Period 2 is marked by a decrease in the lower envelope of $\delta^{34}S$ values of sulfide minerals from approximately 0‰ to approximately −40‰ concomitant with an increase in the upper envelope of $\delta^{34}S$ of sulfate and sulfide minerals from approximately +10‰ to approximately +20‰. This is consistent with increased fractionation with increased availability of sulfate above the limiting value of 200 μM (Habicht et al., 2002). However, it should be noted that others have documented $\delta^{34}S$ fractionation via BSR in an Archean ocean analog that suggest BSR can occur at sulfate concentrations of over an order of magnitude lower values (Crowe et al., 2014), and that kinetic effects can be influenced by reservoir effects at concentrations > 200 μM (Gomes and Hurtgen, 2013), and can also be influenced by the type of sulfate reducer (Bradley et al., 2016). Period 3 (2.45 to 2.00 Ga) has a mode with distinctly lower f_{py} values which are mostly driven by a decline in the average $\delta^{34}S$ values of sample sin this interval, possibly driven by increased oxygen availability during the GOE. During Period 4 the $\delta^{34}S$ values of both sulfate and pyrite rise, though the difference between them remains constant, and consistent with a high value of f_{py}. These high values of f_{py} where then sustained throughout the duration of the Proterozoic and potentially were related to preferential subduction of pyrite and removal of ^{34}S depleted sulfur from the surficial system (Canfield, 2005).

Sulfur isotopic signals are potentially influenced by many biological and abiotic processes, and interpretation of signals found in the rock record requires knowledge of the fractionation associated with each process. Bonds between heavier isotopes are slightly stronger than those between lighter isotopes, and as a result, biological processes preferentially break the bonds of lighter isotopes (in the case of sulfur, selecting ^{32}S over ^{34}S). This isotopic selectivity produces a mass-dependent fractionation. Each biologically mediated pathway can yield a range of isotopic fractionations and on the substrates and products (discussed in detail above). Fractionation is also influenced by resource limitation—decreased fractionation is observed when substrates are only available in limiting amounts. An example of this is biological sulfate reduction (BSR), which is a multi-step process that can produce

sulfides up to 78‰ more ^{32}S depleted than the source sulfate (Brunner and Bernasconi, 2005). However, below a threshold sulfate concentration of ~200 μM, substrate limitation leads to sulfide produced with $\delta^{34}S$ values that are indistinguishable from the sulfate pool (Habicht et al., 2002). Known fractionations for representative reactions involving sulfur compounds are presented in Table 1. Thus, lower sulfate concentrations were likely responsible for curtailed fractionations in Period 1.

An abiotic process that can influence the fractionation of sulfur isotopes is photolysis of SO_2 in the atmosphere. Anomalous $\delta^{33}S$ and $\delta^{36}S$ values discovered in rocks older than 2.4 Ga was explained through experiments exposing SO_2 to ultraviolet radiation (Farquhar et al., 2001). At wavelengths < 220 nm, SO_2 breaks into either elemental sulfur (which is stable as an eight-atom ring, or S_8) or SO_3 which combines with H_2O to form sulfuric acid (H_2SO_4). This process imparts a distinct mass-independent fractionation, with enrichment of ^{33}S and depletion of ^{36}S in S_8 and depletion of ^{33}S and enrichment of ^{36}S in H_2SO_4 (Farquhar et al., 2001). Recent work suggests MIF production can also occur at longer wavelengths of 250 to 350 nm (Whitehill et al., 2013).

8. Interpretation of carbon isotope data

The carbon isotope signal preserved in the rock record is the product of many processes. One process that is directly linked to and driven by the action of life is the isotopic value of carbonates and organic carbon. Mantle-derived carbon has a $\delta^{13}C$ value of −8 to −5‰ (Exley et al., 1986; Javoy et al., 1986; Deines, 2002; Horita and Polyakov, 2015), and is released to the surface as CO_2 via volcanism. Through the study of the better-preserved Phanerozoic rock record and modern carbon cycling systems, a fundamental relationship was observed between removal of carbon from the general ocean DIC pool as organic material preferentially enriched in ^{12}C through biological fixation of CO_2 (discussed in detail above) and concomitant enrichment of the DIC pool in ^{13}C. The resulting ocean DIC values (recorded as carbonates, assuming carbonates precipitated from the DIC pool experience minimal fractionation, < 1‰, Zeebe and Wolf-Gladrow, 2001) are related to the removal of organic carbon through biologic CO_2 fixation by the fractionation imparted through fixation, and the fraction of DIC carbon removed as organic carbon. This relationship is described through the equation:

$$\delta^{13}C_{carb} = \delta^{13}C_{mantle} + f_{org}(\Delta_c)$$

where $\delta^{13}C_{carb}$ is the $\delta^{13}C$ value of the ocean DIC, $\delta^{13}C_{mantle}$ is the $\delta^{13}C$ value of carbon inputs into the surface system (e.g., from the mantle through volcanism), f_{org} is the fraction of total carbon that is removed and sequestered as organic carbon, and Δ_c is the fractionation factor imposed on the organic carbon removed by biologic CO_2 fixation. Assumptions used for this relationship include $\delta^{13}C_{mantle}$ to be ~−5 to −6‰ based on measurements made of modern mid-ocean ridge samples, $\delta^{13}C_{carb}$ values recorded as carbonate minerals precipitated from the ocean, and Δ_c based on a fractionation factor of 25‰ derived from carbon fixation via RuBisCO (such that from a CO_2 source with a $\delta^{13}C$ value of 0‰, biomass produced from CO_2-fixation would have a $\delta^{13}C$ value of −25‰). Using these assumptions, this relationship has been used to describe trends in $\delta^{13}C$ values for carbonates and organic carbon found in Phanerozoic rocks, and to make predictions about the oxygenation of the Earth's surface. Solving for f_{org}, we can use values from the rock record to estimate $\delta^{13}C_{carb}$ and Δ_c to calculate the fraction of organic carbon buried in order to maintain $\delta^{13}C$ values observed. A caveat in estimating the fractionation based on the $\delta^{13}C$ values of organic carbon must be noted when dealing with Archean and Paleoproterozoic biosphere. There are multiple pathways for CO_2-fixation present today, all of which impart fractionation factors that can be dramatically different (Table 2). Furthermore, methanogenesis and methanotrophy likely played larger roles in carbon cycling, potentially shifting buried organic carbon $\delta^{13}C$ values to more negative values. Nonetheless, regardless of the variability of $\delta^{13}C$ fractionations operating at any given time, it is the average of the aggregate organic carbon burial flux that determines the isotopic composition of the ocean atmosphere pool.

This relationship can provide a useful framework for interpreting the fraction of organic carbon buried during the Archean and Paleoproterozoic, based on measured carbonate and organic carbon $\delta^{13}C$ values, and assuming the mantle signal measured today has been similar through earth history. For Period 1, the average carbonate value is 0.7‰, and the majority of organic carbon $\delta^{13}C$ values fall between −25 and −35‰. These values yield f_{org} that are similar to the modern value of 0.20 (Fig. 7). This suggests a burial efficiency during Period 1 that was similar to that of modern-day processes. Period 2 has an average carbonate $\delta^{13}C$ value of −1.1‰, and organic carbon $\delta^{13}C$ values that fall between −30 and −45‰. The calculated f_{org} values for Period 2 are lower than Period 1 (Fig. 7). This suggests increased carbon processing by methanogens and subsequent oxidation and incorporation by methanotrophs (Schidlowski et al., 1983), consistent with increased input of sulfate due to oxidation of pyrite on continental surfaces leading to enhanced organic carbon breakdown by SRO. Period 3 presents two regimes. The first is with an average carbonate $\delta^{13}C$ value of ~0‰ and organic C $\delta^{13}C$ values of that mostly fall between −23 and −39‰. The second is during the Lomagundi-Jatuli carbon isotope excursion (LoJat-CIE), during which most carbonate $\delta^{13}C$ values fall between 0 and +8‰ and organic C $\delta^{13}C$ values of between −24 and −35‰. This shift results in the highest calculated f_{org} value of 0.24, suggesting a shift to less carbon cycling by methanogens/methanotrophs and more effective transfer of fixed carbon to sediments. Period 4 has an average carbonate $\delta^{13}C$ value of −0.3‰ and organic C $\delta^{13}C$ values between −25 and −34‰ giving f_{org} values 0.15. The model by which we calculate f_{org} is the simplest possible one, and thus represents the baseline for the interpretation of the carbon isotopic record. Other models have been proposed, most notably ones that incorporate a burial flux of isotopically reduced carbonate. One hypothesis involves carbonation of basalts in mid-ocean ridges in an isotopically stratified ocean (Bjerrum and Canfield, 2004), but the validity of this hypothesis has been challenged (e.g., Fischer et al., 2009). Another model involves precipitation of authigenic carbonates in sediments during anaerobic respiration of carbon (Schrag et al., 2013). In both of these models a fraction of the organic carbon buried is oxidized and incorporated into the carbonate burial flux thus leading to an isotopically depleted signature of that carbonate flux. The net result is a transfer of isotopically light carbon from the organic carbon burial flux to the carbonate burial flux, Given sufficient magnitude this type of carbonate burial could lead to a high value of $\delta^{13}C_{carb}$ (in continental shelf sediments) even at relatively low rates of organic carbon burial. Presently, constraints on the magnitude of this flux are lacking, and thus the calculation provided here should be taken as a conservative upper envelope of possible values. If isotopically depleted carbonates precipitated in sediment pore space were an important component of the ancient carbon cycle, then the f_{org} values calculate here would be proportionately lower.

The effects of alteration on the organic carbon $\delta^{13}C$ signal resulting from increasing metamorphism of sedimentary rocks will drive a shift towards the positive and thus interpretation of organic carbon $\delta^{13}C$ values is not straightforward (Hayes et al., 1983). To quantify this effect, H:C ratios of kerogen in Archean and Proterozoic samples linked to metamorphic facies can be used to estimate the alteration of the $\delta^{13}C$ signal in the older samples, ranging from 0 to an increase of up to 10‰ (Hayes et al., 1983). Systematic increase in kerogen $\delta^{13}C$ values with decreasing total organic carbon (TOC) content has also been observed, with $\delta^{13}C$ values increasing by 6‰ for each order of magnitude decrease in TOC. This indicates that low TOC samples with more positive $\delta^{13}C$ values may be a result of extensive loss of the initial organic

carbon deposited, as opposed to low initial organic carbon content with a more positive value. For this compilation, we acknowledge that these effects are likely present, and if they are present and systematic, then the lowest values and the differences between the inorganic and organic C $\delta^{13}C$ values will be greater and more pronounced. As the Isua Greenstone Belt samples have been extremely metamorphosed (to amphibolite facies) and undoubtedly altered (Hayes et al., 1983), we have plotted those analyses within brackets to signify that they should be interpreted with great caution (Fig. 1C, D).

9. Synthesis: interpreting carbon and sulfur isotopes through the Archean and Paleoproterozoic

The isotopic records of carbon and sulfur as well as the evolutionary history of biologically mediated carbon and sulfur cycling discussed above aid in interpreting signals imparted in the rock record by biogeochemical cycles over time represented by the rock record. Below we discuss these data in the framework of the periods defined before. The following synthesis represents the culmination of our interpretations of the patterns we have observed in the compiled data. We acknowledge there are alternative interpretations for many of the signals found in the rock record—the aim of our synthesis is to add to the discourse and help drive further work towards a unified interpretation.

9.1. Period 1: 4.0–2.8 Ga

9.1.1. The beginnings of Earth system dynamics

This 1200 million year period includes a transition from delamination-dominant crustal cycling to subduction-dominant cycling, which increased collisional contact between the early cratons and provided the first avenues for the cycling of surface crustal material and sediments into the mantle (Korenaga, 2013 and references therein). It is presumed that Hadean mafic to ultra-mafic crust under a warm ocean would precipitate a large mass of carbonate material (Coogan and Dosso, 2015), and that carbon would be locked in the surface crust under a delamination-dominant crustal cycling regime (Fig. 6D). A suggested putative first continent ('Itsaqia', Nutman et al., 2015) forming circa 3.6 Ga would be consistent with subduction occurring at that time. Initiation of subduction would then begin the process of recycling the carbon locked in the oceanic crust back into the earth surface system as subduction consumed this early crust. In a subduction-dominant regime, ocean crust is cycled over 100 to 200 Ma timescales while continental material can be stable for billions of years. Thus, the formation of stable continental landmass would have provided stable surface area for the accumulation of carbonate, organic carbon, and pyrite. The increase in preserved crustal thickness during this time is a reflection of the increase in continental land mass (Fig. 6B). Sulfide and sulfate $\delta^{34}S$ values indicate mantle sources dominate the surface sulfur pools (Fig. 1A, B), but changes in the range in sulfide values and the lack of sulfate minerals are suggestive of changes in biological processing, presumably due to the emergence of life and subsequent evolution of enzymes.

Molecular clock analysis supports the hypothesis that methanogenesis evolved during the Eoarchean and anoxygenic photosynthesis sometime during the Paleoarchean (Fig. 8)(Walker, 1977; Wächtershäuser, 1990; Battistuzzi et al., 2004). However, calculating rates of evolution and divergence is complicated and usually results in very wide confidence intervals (Davín et al., 2016). Furthermore, molecular clocks are often linked to geologic proxies, biomarkers, or microfossils. Microfossils are rare and controversial and biomarker and geologic proxies can rarely be tied to a single metabolism or taxonomic group. Regardless, the increased occurrence of BIFs in the rock record following 3.6 Ga (Isley and Abbott, 1999) has been suggested to be due in part to anoxygenic photosynthesis using Fe^{2+} as an electron donor, generating insoluble Fe(III) (e.g., Kappler et al., 2005). Anoxygenic photosynthesis involving the oxidation of sulfide would necessitate the

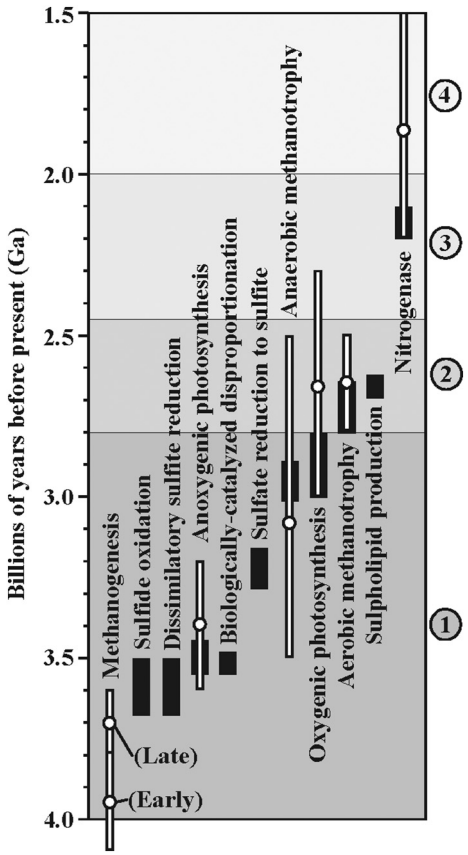

Fig. 8. Predicted onset of sulfur-related metabolisms based on geologic and geochemical evidence (black vertical bars), and estimates from molecular clock calculations (white-filled circles, with white-filled bars representing error range of estimate). Molecular clock estimates of initiation of metabolisms from Battistuzzi et al. (2004) and Boyd et al. (2011).

presence of the molecular machinery required to oxidize sulfide. Also, the presence of small amounts of sulfite as a result of volcanic SO_2 (which would be released from subaerial volcanism) combining with water would provide an oxidized electron donor in a largely reduced ocean. We postulate that sulfide oxidation and dissimilatory sulfite reduction are two of the most ancient sulfur-associated metabolisms, and would likely have developed by 3.5 Ga (Fig. 8). Sulfide $\delta^{34}S$ values prior to 3.6 Ga fall close to the mantle value (Fig. 1A), indicating minimal transferal of a fractionation signal to the rock record, consistent with complete reduction of any oxidized sulfur compounds and with the minimal fractionation associated with sulfide oxidation (Table 1).

Sulfide $\delta^{34}S$ values as negative as $-29.6‰$ with concurrent sulfate $\delta^{34}S$ values ranging from 0.7 to 13.0‰ (Fig. 1A, B) fall within the range of sulfide $\delta^{34}S$ values (-45.2 to $-3.0‰$) and sulfate $\delta^{34}S$ values (1.0 to 30.9‰) expected to result from microbial disproportionation of intermediate redox sulfur compounds such as S^0, $S_2O_3^{2-}$, and SO_3^{2-} (Table 1). This is consistent with microorganisms capable of gaining energy through the transformation of S^0, $S_2O_3^{2-}$, or SO_3^{2-} into sulfide and sulfate around 3.5 Ga, which is in turn consistent with the presence of sulfate minerals after 3.6 Ga. With the ocean sulfate concentration thought to be limiting for biological sulfate reduction, it is likely that there would be little fractionation by sulfate reducers at this time. This onset of microbially mediated disproportionation has been suggested from multiple sulfur isotope work in the 3.5 Ga Dresser Formation (Ueno et al., 2008). Anoxygenic phototrophs could have produced intermediate sulfur compounds (through oxidation of sulfide) that would serve as an energy source for disproportionation. Both anoxygenic photosynthesis and disproportion can generate sulfate as an end

product, and could have provided a source of sulfate in the oceans until the concentrations rose above the energetic threshold for biological sulfate reduction to be viable (i.e., 5 to 77 μM (Ingvorsen and Jørgensen, 1984; Lovley and Klug, 1986)) by 3.25 Ga.

$\Delta^{33}S$ and $\Delta^{36}S$ signals recorded in sulfide and sulfate from ~3.55 to ~3.25 Ga are consistent with photooxidation driving MIF, breaking down SO_2 into SO_3 with negative $\Delta^{33}S$ and positive $\Delta^{36}S$ values and elemental sulfur (as S_8) with positive $\Delta^{33}S$ and negative $\Delta^{36}S$ values (Fig. 2). SO_3 would then combine with H_2O to form sulfate and protons. The muted signal from S_8 indicates the presence of biological sulfur disproportionation, which would result in S_8 being partitioned into both the sulfide and sulfate pools, resulting in a weak MIF signal in sulfate and a stronger MIF signal in sulfide (Fig. 2). It should be noted that recent work has brought into question the dogma of negative $\Delta^{33}S$ and positive $\Delta^{36}S$ values associated with sulfate in MIF signals of the rock record (e.g., Watanabe et al., 2009; Paris et al., 2014).

Under ideal conditions, bacterial sulfate reduction generates fractionations in the end product sulfide that approach − 80‰ (Table 1; Brunner and Bernasconi, 2005). However, at low sulfate concentrations (< 200 μM), isotopic selectivity via biological sulfate reduction is inhibited (e.g., Habicht et al., 2002; Bradley et al., 2016). The disappearance of the $\delta^{34}S$ disproportionation fractionation signal, coupled to a paucity of sulfate minerals in the rock record, all suggest the presence of sulfate reducing organisms after ~3.25 Ga and implies evolution of the first metabolic pathway for reduction of sulfate to sulfite (Fig. 8). This is consistent with an apparent reduction of the $\Delta^{33}S$ signal following ~3.25 Ga suggesting more intense sulfur cycling in the water column was occurring, limiting the potential for transfer of MIF signal to the rock record (Fig. 2A).

Organic carbon $\delta^{13}C$ values during Period 1 (ignoring the Isua values) are consistent with those associated with biomass of modern methanogens (~ − 41 to − 5‰) and anoxygenic phototrophs (~ − 36 to − 9‰) (Schidlowski et al., 1994; Schidlowski, 2001). Molecular clock analysis suggests methanogenesis developed by 3.6 Ga, if not hundreds of millions of years earlier, and that anaerobic methanotrophy developed between 3.5 and 2.5 Ga (Fig. 8). Modern methanotrophic bacterial biomass can have $\delta^{13}C$ values that range from − 85 to − 29‰ (Schidlowski, 2001). The dip in organic C $\delta^{13}C$ values circa 2.9 Ga to values as low as − 44.3‰ would be consistent with the development of methanotrophy at that time as that value is more negative than any modern microbial biomass produced by methanogens or via known carbon fixation pathways (Table 2). A reduction of methane delivery to the atmosphere due to methanotrophy could have reduced methane concentrations in the atmosphere, which may have played a part in initiating the glacial event at that time due to a decrease in the greenhouse effect (Fig. 6D).

Methanotrophy via anaerobic oxidation of methane (AOM) is carried out with sulfate, nitrate, nitrite, Fe^{3+}, or Mn^{4+} as electron acceptors (Beal et al., 2009; Knittel and Boetius, 2009; Ettwig et al., 2010), providing indirect evidence for the production of oxygen in the water column that would be required to generate Mn^{4+} or the oxidized anions nitrate and nitrite. This conclusion is consistent with geochemical proxies that suggest oxygenic photosynthesis was occurring prior to the GOE and as early as 3.0 Ga (Fig. 6D) as well as molecular clock estimates (Fig. 8; Battistuzzi et al., 2004). We postulate that anaerobic methanotrophy evolved around 3.0 to 2.9 Ga, concurrent with oxygenic photosynthesis (Fig. 8). The coupling of methanotrophy to sulfate reduction may have played a part in the paucity of sulfate minerals in the rock record from 3.0 to 2.8 Ga (Fig. 1B) due to complete biological reduction of any produced sulfate.

The first geochemical signs of photosynthetic oxygen production (Fig. 6D, e.g., Anbar et al., 2007; Crowe et al., 2014; Reinhard et al., 2013; Planavsky et al., 2014) are found in rocks following the accumulation of cratons into the first stable continent ('Ur' starting circa 3.0 Ga from the assembly of the Kaapvaal, Dharwar, Bhandara, Singhbhum, and Pilbara cratons; Rogers and Santosh (2003). This suggests the increased volume of shallow sea/restricted basin niche space and stable surface for sediment sequestration was a key component to accelerating the oxidation of the Earth's surface. Overall, there would have been a transition from predominantly ferruginous oceans in the Eoarchean to the first redox-stratified ocean and the potential for local euxinic conditions.

9.2. Period 2: 2.8–2.45 Ga

9.2.1. The buildup to the GOE

Period 2 coincides with a pulse in large igneous province (LIP) production (Fig. 6B) and building of large amounts of crustal material and the formation the first proposed supercontinent ('Kenorland' starting circa 2.7 Ga from the assembly of the Superior, Karelia, Zimbabwe, Kaapvaal, and Pilbara cratons, Rogers and Santosh, 2003; Lubnina and Slabunov, 2011). Coinciding with a period of increased LIP formation (Fig. 6B) is the start of intense BIF formation culminating at the end of this period (Fig. 6C). The area of stable continents at this time was equivalent to ~50% to 75% of modern equivalent (Fig. 6B), providing stable continent surface where sediments could be sequestered and produced shallow basin space where productivity and cycling would have driven isotopic effects in the sulfur and carbon cycles (e.g., Hayes et al., 1983). Basins at this time would have been predominantly populated by anoxygenic phototrophs in the sunlit portion of the water column and methanogens, fermenters and SRO in the deep water and sediments. Oxygenic photosynthesis would have been confined to the upper portions of the water column and/or continental surfaces where environmental conditions permit.

Sulfate minerals are consistently present in the rock record during Period 2, suggesting the sources of sulfate generation are greater than sulfate reducers can consume, reflected in the increasing spread of sulfide $\delta^{34}S$ values (Fig. 1, 3). The increase of sulfate $\delta^{34}S$ values during this time (Fig. 1, 3) suggests there was a persistent source of sulfate to the oceans.

The spread in sulfide and sulfate $\Delta^{33}S$ and $\Delta^{36}S$ signals during this period increased dramatically (Fig. 2). This could be due to an increase in SO_2 delivered to the atmosphere. Increased subaqueous large igneous province generation (Fig. 6B) and ocean floor spreading would have released large amounts of sulfide and Fe^{2+} into the ocean, providing more energy for anoxygenic phototrophs, possibly linked to the increased BIF formation (Fig. 6C). The presence of continental landmass would provide a platform for subaerial large igneous provinces, which would release large amounts of SO_2 into the atmosphere. This pulse in SO_2 would be available to generate a MIF signal (Halevy, 2013), and coupled to the pulse in sulfide from subaqueous volcanism, would contribute to an increase in sulfur present on the earth's surface (though work by Claire et al. (2014) has suggested that additional pathways for MIF signal generation may exist above and beyond that of photolysis of SO_2). This large pulse of sulfur into the surface system would provide a means for transport of MIF signal into the rock record, as sulfur inputs could swamp biological cycling that had dampened the signal at the end of Period 1.

Organic and inorganic $\delta^{13}C$ values become more negative during this period (Fig. 1, 3), possibly due to increased methanotrophy incorporating ^{12}C-enriched CH_4 into organic material and oxidation of organic carbon and CH_4 into isotopically light CO_2 contributing to local DIC pools. The advent of aerobic methanotrophy circa 2.7 Ga is consistent with this interpretation (Fig. 8). The development of aerobic methanotrophy would have produced a new source for isotopically light biomass, and would have reduced the release of methane into the atmosphere, possibly below the threshold for the formation of a hazy atmosphere. With the elimination of the hazy atmosphere, the amount of ultraviolet radiation penetrating the atmosphere would have increased, providing a driver for the formation of MIF signal at a time of increased SO_2 flux into the atmosphere, consistent with the connection between methane collapse and MIF generation (Zahnle et al., 2006).

The increase in stable continent surface and expansion of niche space where oxygenic photosynthesis could persist, coupled to 1.5 Ga of continuous oxidation of the Earth's surface (e.g., hydrogen escape, organic C burial, sulfide burial; Catling and Claire, 2005), led up to conditions where free oxygen could persist in the atmosphere for the first time, heralding the GOE.

9.3. Period 3: 2.45–2.0 Ga

9.3.1. The GOE

Persistent free oxygen in the atmosphere drove rapid chemical weathering of detrital pyrites and uraninites (suggested by the lack of detrital pyrite and uraninite mineral grains in sedimentary rocks deposited after ~2.42 Ga, Johnson et al., 2014) and caused precipitation of iron-oxides forming red beds which are found in the rock record as of ~2.4 Ga (Fig. 6D). Oxidation of labile detrital pyrites found in sands and gravels of terrestrial surfaces led to a flush of sulfate into the oceans (e.g., Havig et al., 2017 and references therein), which would expand the role of BSR in geochemical cycling of carbon, but this would be the tip of the iceberg. Reservoirs of pyrite in exposed Archean sedimentary rocks would also be subjected to oxidative weathering (Bekker and Holland, 2012), as well as iron locked in siderite (Bachan and Kump, 2015). Sulfate $\delta^{34}S$ values drop at the beginning of Period 3 then increase to near Phanerozoic values while sulfide $\delta^{34}S$ values become more negative (Fig. 1). This suggests an increase of sulfate delivery to the oceans from oxidation of pyrites with a bulk $\delta^{34}S$ value close to zero and a shift to BSR in non-sulfate limiting conditions (Fig. 1). Sulfide $\delta^{34}S$ values appear to reflect less fractionation from the sulfate $\delta^{34}S$ values in the middle of Period 3, perhaps reflecting a decreasing sulfate pool or a decrease in BSR activity (e.g., Canfield, 2001).

Subaerial LIP production on continents after 2.4 Ga pumped SO_2 into the atmosphere, which was oxidized to sulfate, deposited in the ocean along with the sulfate from oxidative weathering, reduced to pyrite and buried. This resulted in a redox stratified ocean with surface waters that range from oxygenated to euxinic (e.g., Olson et al., 2013) and euxinic deep water, creating conditions that can drive deposition of manganous carbonates (Havig et al., 2015), with the greatest amount of Mn ore (~60% of the total known global ore reserves) deposited following the initiation of the great oxidation event (Fig. 6C), recently constrained to between 2.460 and 2.426 Ga (Gumsley et al., 2017). The nature of ocean redox stratification during the Paleoproterozoic is still debated, with evidence for both euxinic and ferruginous conditions preserved in shales deposited early in the Paleoproterozoic, but only evidence for euxinic conditions later (Planavsky et al., 2011). This may reflect a difference between restricted basins versus deep marine conditions, and the effects of hydrothermal Fe input versus BSR production of sulfide.

Free oxygen would be consumed quickly through oxidation of detrital and sedimentary pyrites on continental surfaces (producing acidified rivers with high sulfate concentrations, Havig et al., 2017) increased sulfide production by SROs, expanding euxinic zones in the ocean which decreased the niche space for oxygenic photosynthesis. A decrease in burial of organic carbon (possibly due to increased SRO activity) may have also contributed to a short-term pause in the rise in oxygen concentration in the atmosphere (attested by the lag in iron retention in soils to ~2.20 Ga, Fig. 6D). Exposed terrestrial mafic material produced near the end of Period 2 is weathered, and could contribute to a drawdown of atmospheric CO_2, which coupled to the reduction in the release of methane to the atmosphere triggered a series of four global glacial events from ~2.45 to 2.25 Ga. It should be noted, though, that there is currently a lack of constraints on Archean and Proterozoic CO_2 outgassing rates.

The continued overall increase in atmospheric oxygen is reflected in the first retention of iron in paleosols at ~2.20 Ga (Fig. 6D). An increase in continental landmass collisions starting ca. 2.1 Ga drove increased weathering of the continental surface which produced increased burial of organic carbon. This is associated with increased sedimentation and increased oxidative weathering inputting more P into the ocean. More P in the ocean would drive primary production at a time when nitrogen fixation, via the nitrogenase enzyme, has evolved (Fig. 8), reducing nitrogen limitation. Very positive carbonate $\delta^{13}C$ values near the end of the Lomagundi-Jatuli carbon isotope excursion (LoJat-CIE) may reflect the formation of restricted basins associated with the increase in continental surface area and continental breakup prior to the assembly of the supercontinent 'Columbia' (Fig. 6D), creating localized enhancement of the positive isotope excursion effects (e.g., Melezhik et al., 1997; Melezhik et al., 1999; Bekker et al., 2003; Planavsky et al., 2012). Increased oxygen in the atmosphere drove sulfate production as a result of continental weathering. At this time, sulfate concentrations in the oceans may have reached concentrations approaching modern ocean levels (Planavsky et al., 2012; Scott et al., 2014). High sulfate concentrations would lead to increased gypsum deposition, and with over 75% of modern continent landmass present by 2.0 Ga (Fig. 6D), large stable platforms are present for the deposition and removal of large amounts of sulfate.

9.4. Period 4

9.4.1. Earth system quiescence

The assembly of the continents 'Atlantica' (from the West Africa, Brazil, Guyana, Sao Francisco, Rio de la Plata, and Congo/Kasai cratons) and 'Baltica' (from the Baltic and Ukranian shields) circa 2.1 Ga, and the assembly of the supercontinent 'Columbia' circa 2.0 Ga (assembled from the continents Arctica and Baltica, as well as the Penokean, Yavapi, and Mazatzal terrains and probably Eastern Antarctica) (Fig. 6D) resulted in an increase of continental landmass to > 80% of present day, and a pulse in BIF formation between 1.9 and 1.8 Ga (Fig. 6C). It has been suggested that the Sudbury impact at 1.85 Ga (the second largest known impact, producing a ~200 km crater, and coincident with the abrupt cessation of BIF formation) may have been an influencing factor causing ocean mixing and sudden temporary redox homogenization (Slack and Cannon, 2009).

Following the sudden end of the LoJat-CIE around 2.0 Ga, carbon and sulfur isotopic values were stable (Fig. 1). Carbon isotope values were similar to those deposited during the Archean (Fig. 1C, D), and sulfur isotopic values reflect a stable but small ocean sulfate pool that is driven more positive as BSR removed isotopically light sulfur which is buried as pyrite (Fig. 1A, B). A speculative connection between the end of the LoJat-CIE (marked by a massive deposition of organic material that resulted in a "petrified oil field", called the Shunga Event, Medvedev et al., 2009) which coincides with the 2.023 Ga Vredefort impact (forming a ~300 km diameter crater) has been made, suggesting large impacts may cause impacts on the biosphere on scales that can effect global processes (Young, 2013). Similar smaller "petrified oil" deposits have also been found associated with the 1.85 Ga Sudbury impact (Medvedev et al., 2009).

Reduced sulfate concentrations in the oceans caused a collapse in the influence of BSR, allowing methanogens to occupy the water-sediment interface, and increasing the amount of methane released into the water column. Continental weathering buffered atmospheric CO_2, the redox-stratified ocean supported a stable dissolved inorganic carbon-organic carbon-methane feedback loop, and the supercontinent 'Columbia' remained relatively stable until a period of rifting that ended with the reformation of the supercontinent as 'Rodina' circa 1.1 Ga (Roberts, 2013). During this relative geochemical and tectonic quiescence, complex life evolved including nucleated cells (circa 1.5 Ga, Schopf, 1974; Martin and Russell, 2003), macroalgal features (Mesoproterozoic, Xiao and Dong, 2006), and sexual reproduction (circa 1.2 Ga, Butterfield, 2000), setting the stage for the rapid diversification of Ediacaran metasomes and the subsequent Cambrian explosion following the second great oxidation event during the Neoproterozoic.

10. Concluding thoughts

The geochemical upheaval in sulfur and carbon isotopes that characterizes the first half of the Paleoproterozoic lies in stark contrast to the quiescence that typifies the second half. Furthermore, geologic and geochemical evidence for dramatic changes in the oxidation state of the surface environment occur during the first half, with no major changes observed to date in the second half. From this, perhaps it is useful to recognize and signify these differences by dividing the Paleoproterozoic into two separate Eras, with the Paleoproterozoic encompassing the Orosirian and Statherian Periods (from 2.05 to 1.6 Ga), and a new Eoproterozoic Era encompassing the Siderian and Rhyacian Periods (from 2.45 to 2.05 Ga), and bringing the boundary between the Proterozoic and Archean to ~2.45 Ga (in light of the recent age dates constraining the great oxidation event by Gumsley et al., 2017).

We argue for an intimate connection between the biosphere and sulfur isotope signals preserved in the rock record. While the influence of biological processes on $\delta^{34}S$ signals of sulfide and sulfate are somewhat constrained by pure culture and environmental work, more work is needed on a greater range of pure culture isolates as well as environmental samples to interpret the effects on preservation of $\delta^{34}S$ signals that result from complex sulfur cycling in natural systems, especially in the face of sulfate limitation. Furthermore, assumptions made on preservation of $\Delta^{33}S$ and $\Delta^{36}S$ signals (generated by MIF processes) in the rock record are done in an absence of experimental work to elucidate the effects of biological sulfur metabolisms on processing and altering sulfur compounds that carry MIF signals, providing an open and exciting avenue for exploration.

While the views expressed in this work are not presumed to be definitive, and certainly not the final word on the sulfur-carbon isotope system in the Archean and Paleoproterozoic, we hope that what we have presented will provide some food for thought, and will aid in efforts to produce a holistic, multi-discipline synthesis of the development of the earth-biosphere system that better integrates the influences of life on the earth system. This is a time of rapid progression of thought and the accumulation of massive geochemical datasets, coincident with the explosion of molecular capabilities and novel work being done in molecular microbiology and ecology. It is an exciting time that will yield new paradigms as the old are turned on their ear.

Acknowledgements

JRH would like to thank the Penn State Astrobiology Research Center for generous support, the University of Cincinnati for support, and Dr. Chris House for support and encouragement. TLH graciously acknowledges support from the University of Cincinnati.

References

Anbar, A.D., Duan, Y., Lyons, T.W., Arnold, G.L., Kendall, B., Creaser, R.A., Kaufman, A.J., Gordon, G.W., Scott, C., Garvin, J., Buick, R., 2007. A whiff of oxygen before the great oxidation event? Science 317 (5846), 1903–1906.

Bachan, A., Kump, L.R., 2015. The rise of oxygen and siderite oxidation during the Lomagundi event. Proc. Natl. Acad. Sci. 112 (21), 6562–6567.

Badger, M.R., Bek, E.J., 2008. Multiple Rubisco forms in proteobacteria: their functional significance in relation to CO_2 acquisition by the CBB cycle. J. Exp. Bot. 59 (7), 1525–1541.

Bar-Even, A., Noor, E., Milo, R., 2011. A survey of carbon fixation pathways through a quantitative lens. J. Exp. Bot. 63 (6), 2325–2342.

Battistuzzi, F.U., Feijao, A., Hedges, S.B., 2004. A genomic timescale of prokaryote evolution: insights into the origin of methanogenesis, phototrophy, and the colonization of land. BMC Evol. Biol. 4 (1), 1.

Beal, E.J., House, C.H., Orphan, V.J., 2009. Manganese- and iron-dependent marine methane oxidation. Science 325, 184–187. http://dx.doi.org/10.1126/science.1169984.

Bekker, A., Holland, H.D., 2012. Oxygen overshoot and recovery during the early Paleoproterozoic. Earth Planet. Sci. Lett. 317, 295–304.

Bekker, A., Karhu, J.A., Eriksson, K.A., Kaufman, A.J., 2003. Chemostratigraphy of Paleoproterozoic carbonate successions of the Wyoming Craton: tectonic forcing of biogeochemical change? Precambrian Res. 120 (3), 279–325.

Bekker, A., Slack, J.F., Planavsky, N., Krapež, B., Hofmann, A., Konhauser, K.O., Rouxel, O.J., 2010. Iron formation: the sedimentary product of a complex interplay among mantle, tectonic, oceanic, and biospheric processes. Econ. Geol. 105 (3), 467–508.

Berg, I.A., 2011. Ecological aspects of the distribution of different autotrophic CO_2 fixation pathways. Appl. Environ. Microbiol. 77 (6), 1925–1936.

Berg, I.A., Kockelkorn, D., Ramos-Vera, W.H., Say, R.F., Zarzycki, J., Hügler, M., ... Fuchs, G., 2010. Autotrophic carbon fixation in archaea. Nat. Rev. Microbiol. 8 (6), 447–460.

Bjerrum, C.J., Canfield, D.E., 2004. New insights into the burial history of organic carbon on the early earth. Geochem. Geophys. Geosyst. 5 (8).

Borrel, G., Adam, P.S., Gribaldo, S., 2016. Methanogenesis and the Wood–Ljungdahl pathway: an ancient, versatile, and fragile association. Genome Biol. Evol. 8 (6), 1706–1711.

Botsch, K.C., Conrad, R., 2011. Fractionation of stable carbon isotopes during anaerobic production and degradation of propionate in defined microbial cultures. Org. Geochem. 42 (3), 289–295.

Boucher, Y., Douady, C.J., Papke, R.T., Walsh, D.A., Boudreau, M.E.R., Nesbø, C.L., ... Doolittle, W.F., 2003. Lateral gene transfer and the origins of prokaryotic groups. Annu. Rev. Genet. 37 (1), 283–328.

Boyd, E.S., Hamilton, T.L., Peters, J.W., 2011. An alternative path for the evolution of biological nitrogen fixation. Front. Microbiol. 2, 205.

Böttcher, M.E., Thamdrup, B., Gehre, M., Theune, A., 2005. 34S/32S and 18O/16O fractionation during sulfur disproportionation by Desulfobulbus propionicus. Geomicrobiol J. 22 (5), 219–226.

Bradley, A.S., Leavitt, W.D., Schmidt, M., Knoll, A.H., Girguis, P.R., Johnston, D.T., 2016. Patterns of sulfur isotope fractionation during microbial sulfate reduction. Geobiology 14 (1), 91–101.

Brunner, B., Bernasconi, S.M., 2005. A revised isotope fractionation model for dissimilatory sulfate reduction in sulfate reducing bacteria. Geochim. Cosmochim. Acta 69 (20), 4759–4771.

Bryan, S.E., Ernst, R.E., 2008. Revised definition of large igneous provinces (LIPs). Earth Sci. Rev. 86 (1), 175–202.

Budai, J.M., Martini, A.M., Walter, L.M., Ku, T.C.W., 2002. Fracture-fill calcite as a record of microbial methanogenesis and fluid migration: a case study from the Devonian Antrim Shale, Michigan Basin. Geofluids 2 (3), 163–183.

Butterfield, N.J., 2000. *Bangiomorpha pubescens* n. gen., n. sp.: implications for the evolution of sex, multicellularity, and the Mesoproterozoic/Neoproterozoic radiation of eukaryotes. Paleobiology 26 (3), 386–404.

Canfield, D.E., 2001. Isotope fractionation by natural populations of sulfate-reducing bacteria. Geochim. Cosmochim. Acta 65 (7), 1117–1124.

Canfield, D.E., 2005. The early history of atmospheric oxygen: homage to Robert M. Garrels. Annu. Rev. Earth Planet. Sci. 33, 1–36.

Canfield, D.E., Raiswell, R., 1999. The evolution of the sulfur cycle. Am. J. Sci. 299 (7–9), 697–723.

Canfield, D.E., Rosing, M.T., Bjerrum, C., 2006. Early anaerobic metabolisms. Philos. Trans. R. Soc. Lond. B Biol. Sci. 361 (1474), 1819–1836.

Catling, D.C., Claire, M.W., 2005. How Earth's atmosphere evolved to an oxic state: a status report. Earth Planet. Sci. Lett. 237 (1), 1–20.

Claire, M.W., Kasting, J.F., Domagal-Goldman, S.D., Stüeken, E.E., Buick, R., Meadows, V.S., 2014. Modeling the signature of sulfur mass-independent fractionation produced in the Archean atmosphere. Geochim. Cosmochim. Acta 141, 365–380.

Collerson, K.D., Kamber, B.S., 1999. Evolution of the continents and the atmosphere inferred from Th-U-Nb systematics of the depleted mantle. Science 283 (5407), 1519–1522.

Condie, K.C., 2014. Growth of continental crust: a balance between preservation and recycling. Mineral. Mag. 78 (3), 623–638.

Conrad, R., 2005. Quantification of methanogenic pathways using stable carbon isotopic signatures: a review and a proposal. Org. Geochem. 36 (5), 739–752.

Conrad, R., Claus, P., Chidthaisong, A., Lu, Y., Scavino, A.F., Liu, Y., Angel, R., Galand, P.E., Casper, P., Guerin, F., Enrich-Prast, A., 2014. Stable carbon isotope biogeochemistry of propionate and acetate in methanogenic soils and lake sediments. Org. Geochem. 73, 1–7.

Coogan, L.A., Dosso, S.E., 2015. Alteration of ocean crust provides a strong temperature dependent feedback on the geological carbon cycle and is a primary driver of the Sr-isotopic composition of seawater. Earth Planet. Sci. Lett. 415, 38–46.

Costa, K.C., Leigh, J.A., 2014. Metabolic versatility in methanogens. Curr. Opin. Biotechnol. 29, 70–75.

Crowe, S.A., Jones, C., Katsev, S., Magen, C., O'Neill, A.H., Sturm, A., Canfield, D.E., Haffner, G.D., Mucci, A., Sundby, B., Fowle, D.A., 2008. Photoferrotrophs thrive in an Archean Ocean analogue. Proc. Natl. Acad. Sci. 105 (41), 15938–15943.

Crowe, S.A., Paris, G., Katsev, S., Jones, C., Kim, S.T., Zerkle, A.L., Nomosatryo, S., Fowle, D.A., Adkins, J.F., Sessions, A.L., Farquhar, J., 2014. Sulfate was a trace constituent of Archean seawater. Science 346 (6210), 735–739.

Cypionka, H., Smock, A.M., Böttcher, M.E., 1998. A combined pathway of sulfur compound disproportionation in Desulfovibrio desulfuricans. FEMS Microbiol. Lett. 166 (2), 181–186.

Davín, A., Szöllosi, G.J., Tannier, E., Boussau, B., Daubin, V., 2016. Dating with transfers. In: Journées ouvertes Bilogie Informatique Mathématiques.

Deines, P., 2002. The carbon isotope geochemistry of mantle xenoliths. Earth Sci. Rev. 58 (3), 247–278.

Dhuime, B., Wuestefeld, A., Hawkesworth, C.J., 2015. Emergence of modern continental crust about 3 billion years ago. Nat. Geosci. 8 (7), 552–555.

Domagal-Goldman, S.D., Kasting, J.F., Johnston, D.T., Farquhar, J., 2008. Organic haze, glaciations and multiple sulfur isotopes in the Mid-Archean Era. Earth Planet. Sci. Lett. 269 (1), 29–40.

Drake, H., Åström, M.E., Heim, C., Broman, C., Åström, J., Whitehouse, M., Ivarsson, M., Siljeström, S., Sjövall, P., 2015. Extreme ^{13}C depletion of carbonates formed during

oxidation of biogenic methane in fractured granite. Nat. Commun. 6.
Ellis, R.J., 1979. Most abundant protein in the world. Trends Biochem. Sci. 4, 241–244.
Ettwig, K.F., Butler, M.K., Le Paslier, D., Pelletier, E., Mangenot, S., Kuypers, M.M., Schreiber, F., Dutihl, B.E., Zedelius, J., De Beer, D., Gloerich, J., 2010. Nitrite-driven anaerobic methane oxidation by oxygenic bacteria. Nature 464 (7288), 543–548.
Evans, P.N., Parks, D.H., Chadwick, G.L., Robbins, S.J., Orphan, V.J., Golding, S.D., Tyson, G.W., 2015. Methane metabolism in the archaeal phylum Bathyarchaeota revealed by genome-centric metagenomics. Science 350 (6259), 434–438.
Exley, R.A., Mattey, D.P., Clague, D.A., Pillinger, C.T., 1986. Carbon isotope systematics of a mantle "hotspot": a comparison of Loihi Seamount and MORB glasses. Earth Planet. Sci. Lett. 78 (2), 189–199.
Farquhar, J., Savarino, J., Airieau, S., Thiemens, M.H., 2001. Observation of wavelength-sensitive mass-independent sulfur isotope effects during SO_2 photolysis: implications for the early atmosphere. J. Geophys. Res. Planets 106 (E12), 32829–32839.
Fischer, W.W., Schroeder, S., Lacassie, J.P., Beukes, N.J., Goldberg, T., Strauss, H., Horstmann, U.E., Schrag, D.P., Knoll, A.H., 2009. Isotopic constraints on the Late Archean carbon cycle from the Transvaal Supergroup along the western margin of the Kaapvaal Craton, South Africa. Precambrian Res. 169 (1), 15–27.
Frei, R., Gaucher, C., Poulton, S.W., Canfield, D.E., 2009. Fluctuations in Precambrian atmospheric oxygenation recorded by chromium isotopes. Nature 461 (7261), 250.
Frigaard, N.U., Bryant, D.A., 2008. Genomic and evolutionary perspectives on sulfur metabolism in green sulfur bacteria. In: Microbial Sulfur Metabolism. Springer, Berlin Heidelberg, pp. 60–76.
Frigaard, N.-U., Dahl, C., 2009. Sulfur metabolism in phototrophic sulfur bacteria. In: Poole, R.K. (Ed.), Advances in Microbial Physiology. London: Academic Press, pp. 103–200.
Fry, B., Gest, H., Hayes, J.M., 1985. Isotope effects associated with the anaerobic oxidation of sulfite and thiosulfate by the photosynthetic bacterium, *Chromatium vinosum*. FEMS Microbiol. Lett. 27 (2), 227–232.
Fry, B., Cox, J., Gest, H., Hayes, J.M., 1986. Discrimination between ^{34}S and ^{32}S during bacterial metabolism of inorganic sulfur compounds. J. Bacteriol. 165 (1), 328–330.
Fry, B., Ruf, W., Gest, H., Hayes, J.M., 1988. Sulfur isotope effects associated with oxidation of sulfide by O_2 in aqueous solution. Chem. Geol. Isot. Geosci. Sect. 73 (3), 205–210.
Fuchs, G., 2011. Alternative pathways of carbon dioxide fixation: insights into the early evolution of life? Annu. Rev. Microbiol. 65, 631–658.
Fuchs, G., Thauer, R., Ziegler, H., Stichler, W., 1979. Carbon isotope fractionation by Methanobacterium thermoautotrophicum. Arch. Microbiol. 120 (2), 135–139.
Fuseler, K., Krekeler, D., Sydow, U., Cypionka, H., 1996. A common pathway of sulfide oxidation by sulfate-reducing bacteria. FEMS Microbiol. Lett. 144 (2–3), 129–134.
Goevert, D., Conrad, R., 2008. Carbon isotope fractionation by sulfate-reducing bacteria using different pathways for the oxidation of acetate. Environ. Sci. Technol. 42 (21), 7813–7817.
Goevert, D., Conrad, R., 2009. Effect of substrate concentration on carbon isotope fractionation during acetoclastic methanogenesis by *Methanosarcina barkeri* and *M. acetivorans* and in rice field soil. Appl. Environ. Microbiol. 75 (9), 2605–2612.
Gomes, M.L., Hurtgen, M.T., 2013. Sulfur isotope systematics of a euxinic, low-sulfate lake: evaluating the importance of the reservoir effect in modern and ancient oceans. Geology 41 (6), 663–666.
Gregersen, L.H., Bryant, D.A., Frigaard, N.U., 2011. Mechanisms and evolution of oxidative sulfur metabolism in green sulfur bacteria. Front. Microbiol. 2, 116.
Grein, F., Ramos, A.R., Venceslau, S.S., Pereira, I.A., 2013. Unifying concepts in anaerobic respiration: insights from dissimilatory sulfur metabolism. BBA-Bioenergetics 1827 (2), 145–160.
Gross, G.A., 1980. A classification of iron formations based on depositional environments. Can. Mineral. 18 (2), 215–222.
Gumsley, A.P., Chamberlain, K.R., Bleeker, W., Söderlund, U., de Kock, M.O., Larsson, E.R., Bekker, A., 2017. Timing and tempo of the Great Oxidation Event. Proc. Natl. Acad. Sci. 114 (8), 1811–1816.
Habicht, K.S., Canfield, D.E., 1997. Sulfur isotope fractionation during bacterial sulfate reduction in organic-rich sediments. Geochim. Cosmochim. Acta 61 (24), 5351–5361.
Habicht, K.S., Canfield, D.E., Rethmeier, J., 1998. Sulfur isotope fractionation during bacterial reduction and disproportionation of thiosulfate and sulfite. Geochim. Cosmochim. Acta 62 (15), 2585–2595.
Habicht, K.S., Gade, M., Thamdrup, B., Berg, P., Canfield, D.E., 2002. Calibration of sulfate levels in the Archean ocean. Science 298 (5602), 2372–2374.
Halevy, I., 2013. Production, preservation, and biological processing of mass-independent sulfur isotope fractionation in the Archean surface environment. Proc. Natl. Acad. Sci. 110 (44), 17644–17649.
Hannisdal, B., Peters, S.E., 2011. Phanerozoic Earth system evolution and marine biodiversity. Science 334 (6059), 1121–1124.
Haqq-Misra, J.D., Domagal-Goldman, S.D., Kasting, P.J., Kasting, J.F., 2008. A revised, hazy methane greenhouse for the Archean earth. Astrobiology 8 (6), 1127–1137.
Hatch, F.H., Rastall, R.H., 1965. Petrology of the Sedimentary Rocks. vol. 2 T. Murby.
Havig, J.R., Raymond, J., Meyer-Dombard, D.A.R., Zolotova, N., Shock, E.L., 2011. Merging isotopes and community genomics in a siliceous sinter-depositing hot spring. J. Geophys. Res. Biogeosci. 116 (G1).
Havig, J.R., McCormick, M.L., Hamilton, T.L., Kump, L.R., 2015. The behavior of biologically important trace elements across the oxic/euxinic transition of meromictic Fayetteville Green Lake, New York, USA. Geochim. Cosmochim. Acta 165, 389–406.
Havig, J.R., Hamilton, T.L., Grettenberger, C., 2017. Geochemistry and microbial community composition across a range of acid mine drainage impact and implications for the Neoarchean-Paleoproterozoic transition. J. Geophys. Res. Biogeosci. 122.
Hayes, J.M., Wedeking, K.W., Kaplan, I.R., 1983. Precambrian organic geochemistry, preservation of the record. In: Schopf, J.W. (Ed.), Earth's Earliest Biosphere: Its Origin and Evolution. Princeton University Press, Princeton, NJ, pp. 93–133 (Print).
Hayes, J.M., Strauss, H., Kaufman, A.J., 1999. The abundance of ^{13}C in marine organic matter and isotopic fractionation in the global biogeochemical cycle of carbon during the past 800 Ma. Chem. Geol. 161 (1), 103–125.
Heuer, V., Elvert, M., Tille, S., Krummen, M., Mollar, X.P., Hmelo, L.R., Hinrichs, K.U., 2006. Online $\delta^{13}C$ analysis of volatile fatty acids in sediment/porewater systems by liquid chromatography-isotope ratio-mass spectrometry. Limnol. Oceanogr. Methods 4, 346–357.
Hoffman, P.F., 2013. The great oxidation and a Siderian snowball Earth: MIF-S based correlation of Paleoproterozoic glacial epochs. Chem. Geol. 362, 143–156.
Holland, H.D., 1994. Early Proterozoic atmospheric change. In: Early Life on Earth. vol. 84. Columbia University Press, New York, pp. 237–244.
Holland, H.D., 2009. Why the atmosphere became oxygenated: a proposal. Geochim. Cosmochim. Acta 73 (18), 5241–5255.
Holo, H., Sirevåg, R., 1986. Autotrophic growth and CO_2 fixation of *Chloroflexus aurantiacus*. Arch. Microbiol. 145 (2), 173–180.
Horita, J., Berndt, M.E., 1999. Abiogenic methane formation and isotopic fractionation under hydrothermal conditions. Science 285 (5430), 1055–1057.
Horita, J., Polyakov, V.B., 2015. Carbon-bearing iron phases and the carbon isotope composition of the deep Earth. Proc. Natl. Acad. Sci. 112 (1), 31–36.
House, C.H., Schopf, J.W., Stetter, K.O., 2003. Carbon isotopic fractionation by Archaeans and other thermophilic prokaryotes. Org. Geochem. 34 (3), 345–356.
Hulston, J.R., Thode, H.G., 1965. Variations in the S33, S34, and S36 contents of meteorites and their relation to chemical and nuclear effects. J. Geophys. Res. 70 (14), 3475–3484.
Ingvorsen, K., Jørgensen, B.B., 1984. Kinetics of sulfate uptake by freshwater and marine species of *Desulfovibrio*. Arch. Microbiol. 139 (1), 61–66.
Isley, A.E., Abbott, D.H., 1999. Plume-related mafic volcanism and the deposition of banded iron formation. J. Geophys. Res. Solid Earth 104 (B7), 15461–15477.
Ivanovsky, R.N., Krasilnikova, E.N., Fal, Y.I., 1993. A pathway of the autotrophic CO_2 fixation in *Chloroflexus aurantiacus*. Arch. Microbiol. 159 (3), 257–264.
James, H.L., 1954. Sedimentary facies of iron-formation. Econ. Geol. 49 (3), 235–293.
Jamieson, J.W., Wing, B.A., Farquhar, J., Hannington, M.D., 2013. Neoarchaean seawater sulphate concentrations from sulphur isotopes in massive sulphide ore. Nat. Geosci. 6 (1), 61–64.
Janssen, P.H., Schuhmann, A., Bak, F., Liesack, W., 1996. Disproportionation of inorganic sulfur compounds by the sulfate-reducing bacterium *Desulfocapsa thiozymogenes* gen. nov., sp. nov. Arch. Microbiol. 166 (3), 184–192.
Jaun, B., Thauer, R.K., 2007. Methyl-coenzyme M reductase and its nickel corphin coenzyme F430 in methanogenic archaea. In: Nickel and Its Surprising Impact in Nature. 2. pp. 323–356.
Javoy, M., Pineau, F., Delorme, H., 1986. Carbon and nitrogen isotopes in the mantle. Chem. Geol. 57 (1–2), 41–62.
Johnson, J.E., Webb, S.M., Thomas, K., Ono, S., Kirschvink, J.L., Fischer, W.W., 2013. Manganese-oxidizing photosynthesis before the rise of cyanobacteria. Proc. Natl. Acad. Sci. 110 (28), 11238–11243.
Johnson, J.E., Gerpheide, A., Lamb, M.P., Fischer, W.W., 2014. O_2 constraints from Paleoproterozoic detrital pyrite and uraninite. Geol. Soc. Am. Bull. 126 (5–6), 813–830.
Johnson, T.E., Brown, M., Gardiner, N.J., Kirkland, C.L., Smithies, R.H., 2017. Earth's first stable continents did not form by subduction. Nature 543 (7644), 239–242.
Kanzaki, Y., Murakami, T., 2016. Estimates of atmospheric O_2 in the Paleoproterozoic from paleosols. Geochim. Cosmochim. Acta 174, 263–290.
Kappler, A., Pasquero, C., Konhauser, K.O., Newman, D.K., 2005. Deposition of banded iron formations by anoxygenic phototrophic Fe(II)-oxidizing bacteria. Geology 33 (11), 865–868.
Kasting, J.F., 2013. What caused the rise of atmospheric O_2? Chem. Geol. 362, 13–25.
Keller, C.B., Schoene, B., 2012. Statistical geochemistry reveals disruption in secular lithospheric evolution about 2.5 G yr ago. Nature 485 (7399), 490–493.
Klatt, C.G., Wood, J.M., Rusch, D.B., Bateson, M.M., Hamamura, N., Heidelberg, J.F., Grossman, A.R., Bhaya, D., Cohan, F.M., Kühl, M., Bryant, D.A., 2011. Community ecology of hot spring cyanobacterial mats: predominant populations and their functional potential. ISME J. 5 (8), 1262.
Klatt, C.G., Inskeep, W.P., Herrgard, M.J., Jay, Z.J., Rusch, D.B., Tringe, S.G., Parenteau, M.N., Ward, D.M., Boomer, S.M., Bryant, D.A., Miller, S.R., 2013. Community structure and function of high-temperature chlorophototrophic microbial mats inhabiting diverse geothermal environments. Front. Microbiol. 4.
Kletzin, A., Urich, T., Müller, F., Bandeiras, T.M., Gomes, C.M., 2004. Dissimilatory oxidation and reduction of elemental sulfur in thermophilic archaea. J. Bioenerg. Biomembr. 36 (1), 77–91.
Knittel, K., Boetius, A., 2009. Anaerobic oxidation of methane: progress with an unknown process. Annu. Rev. Microbiol. 63, 311–334.
Korenaga, J., 2013. Initiation and evolution of plate tectonics on Earth: theories and observations. Annu. Rev. Earth Planet. Sci. 41, 117–151.
Kump, L.R., 2008. The rise of atmospheric oxygen. Nature 451 (7176), 277–278.
Kump, L.R., Barley, M.E., 2007. Increased subaerial volcanism and the rise of atmospheric oxygen 2.5 billion years ago. Nature 448 (7157), 1033–1036.
Labidi, J., Cartigny, P., Birck, J.L., Assayag, N., Bourrand, J.J., 2012. Determination of multiple sulfur isotopes in glasses: a reappraisal of the MORB $\delta^{34}S$. Chem. Geol. 334, 189–198.
Leavitt, W.D., Halevy, I., Bradley, A.S., Johnston, D.T., 2013. Influence of sulfate reduction rates on the Phanerozoic sulfur isotope record. Proc. Natl. Acad. Sci. 110 (28), 11244–11249.
Lever, M.A., 2016. A new era of methanogenesis research. Trends Microbiol. 24 (2), 84–86.
Lever, M.A., Rouxel, O., Alt, J.C., Shimizu, N., Ono, S., Coggon, R.M., Shanks, W.C., Lapham, L., Elvert, M., Prieto-Mollar, X., Hinrichs, K.U., 2013. Evidence for microbial

carbon and sulfur cycling in deeply buried ridge flank basalt. Science 339 (6125), 1305–1308.
Lin, Z., Sun, X., Peckmann, J., Lu, Y., Xu, L., Strauss, H., Zhou, H., Gong, J., Lu, H., Teichert, B.M., 2016. How sulfate-driven anaerobic oxidation of methane affects the sulfur isotopic composition of pyrite: a SIMS study from the South China Sea. Chem. Geol. 440, 26–41.
Londry, K.L., Des Marais, D.J., 2003. Stable carbon isotope fractionation by sulfate-reducing bacteria. Appl. Environ. Microbiol. 69 (5), 2942–2949.
Londry, K.L., Dawson, K.G., Grover, H.D., Summons, R.E., Bradley, A.S., 2008. Stable carbon isotope fractionation between substrates and products of *Methanosarcina barkeri*. Org. Geochem. 39 (5), 608–621.
Lovelock, J., 1988. The Ages of Gaia: A Biography of Our Living Planet. W.W. Norton & Company, New York.
Lovley, D.R., Klug, M.J., 1986. Model for the distribution of sulfate reduction and methanogenesis in freshwater sediments. Geochim. Cosmochim. Acta 50 (1), 11–18.
Lubnina, N.V., Slabunov, A.I., 2011. Reconstruction of the Kenorland supercontinent in the Neoarchean based on paleomagnetic and geological data. Mosc. Univ. Geol. Bull. 66 (4), 242–249.
Lyons, T.W., Reinhard, C.T., Planavsky, N.J., 2014. The rise of oxygen in Earth/'s early ocean and atmosphere. Nature 506 (7488), 307–315.
Machel, H.G., 2001. Bacterial and thermochemical sulfate reduction in diagenetic settings—old and new insights. Sediment. Geol. 140 (1), 143–175.
Marcia, M., Ermler, U., Peng, G., Michel, H., 2010. A new structure-based classification of sulfide: quinone oxidoreductases. Proteins: Struct., Funct., Bioinf. 78 (5), 1073–1083.
Martin, W., Russell, M.J., 2003. On the origins of cells: a hypothesis for the evolutionary transitions from abiotic geochemistry to chemoautotrophic prokaryotes, and from prokaryotes to nucleated cells. Philos. Trans. R. Soc. Lond. B Biol. Sci. 358 (1429), 59–85.
Martin, W., Baross, J., Kelley, D., Russell, M.J., 2008. Hydrothermal vents and the origin of life. Nat. Rev. Microbiol. 6 (11), 805–814.
Maynard, J.B., 2010. The chemistry of manganese ores through time: a signal of increasing diversity of earth-surface environments. Econ. Geol. 105 (3), 535–552.
McCollom, T.M., Shock, E.L., 1997. Geochemical constraints on chemolithoautotrophic metabolism by microorganisms in seafloor hydrothermal systems. Geochim. Cosmochim. Acta 61 (20), 4375–4391.
McNevin, D.B., Badger, M.R., Whitney, S.M., von Caemmerer, S., Tcherkez, G.G., Farquhar, G.D., 2007. Differences in carbon isotope discrimination of three variants of D-ribulose-1,5-bisphosphate carboxylase/oxygenase reflect differences in their catalytic mechanisms. J. Biol. Chem. 282 (49), 36068–36076.
Medvedev, P.V., Melezhik, V.A., Filippov, M.M., 2009. Palaeoproterozoic petrified oil field (Shunga event). Paleontol. J. 43 (8), 972.
Melezhik, V., Fallick, A., Clark, T., 1997. Two billion year old isotopically heavy carbon: evidence from the Labrador Trough, Canada. Can. J. Earth Sci. 34 (3), 271–285.
Melezhik, V.A., Fallick, A.E., Medvedev, P.V., Makarikhin, V.V., 1999. Extreme ^{13}Ccarb enrichment in ca. 2.0 Ga magnesite–stromatolite–dolomite–red beds' association in a global context: a case for the world-wide signal enhanced by a local environment. Earth Sci. Rev. 48 (1), 71–120.
Melezhik, V.A., Fallick, A.E., Martin, A.P., Condon, D.J., Kump, L.R., Brasier, A.T., Salminen, P.E., 2013. 7.3 the Palaeoproterozoic perturbation of the global carbon cycle: the Lomagundi-Jatuli isotopic event. In: Reading the Archive of Earth's Oxygenation. Springer, Berlin Heidelberg, pp. 1111–1150.
Mitchell, R.L., Sheldon, N.D., 2016. Sedimentary provenance and weathering processes in the 1.1 Ga Midcontinental Rift of the Keweenaw Peninsula, Michigan, USA. Precambrian Res. 275, 225–240.
Müller, F.H., Bandeiras, T.M., Urich, T., Teixeira, M., Gomes, C.M., Kletzin, A., 2004. Coupling of the pathway of sulphur oxidation to dioxygen reduction: characterization of a novel membrane-bound thiosulphate: quinone oxidoreductase. Mol. Microbiol. 53 (4), 1147–1160.
Muyzer, G., Stams, A.J., 2008. The ecology and biotechnology of sulphate-reducing bacteria. Nat. Rev. Microbiol. 6 (6), 441–454.
Nelson, D.C., Castenholz, R.W., 1981. Use of reduced sulfur compounds by Beggiatoa sp. J. Bacteriol. 147, 140–154.
Neuendorf, K.K., 2005. Glossary of Geology. Springer Science & Business Media.
Nutman, A.P., Bennett, V.C., Friend, C.R., 2015. Proposal for a continent 'Itsaqia'amalgamated at 3.66 Ga and rifted apart from 3.53 Ga: initiation of a Wilson cycle near the start of the rock record. Am. J. Sci. 315 (6), 509–536.
Olson, J.M., 2006. Photosynthesis in the Archean era. Photosynth. Res. 88 (2), 109–117.
Olson, S.L., Kump, L.R., Kasting, J.F., 2013. Quantifying the areal extent and dissolved oxygen concentrations of Archean oxygen oases. Chem. Geol. 362, 35–43.
Paris, G., Adkins, J.F., Sessions, A.L., Webb, S.M., Fischer, W.W., 2014. Neoarchean carbonate–associated sulfate records positive Δ33S anomalies. Science 346 (6210), 739–741.
Pellerin, A., Bui, T.H., Rough, M., Mucci, A., Canfield, D.E., Wing, B.A., 2015. Mass-dependent sulfur isotope fractionation during reoxidative sulfur cycling: a case study from Mangrove Lake, Bermuda. Geochim. Cosmochim. Acta 149, 152–164.
Penning, H., Conrad, R., 2006. Carbon isotope effects associated with mixed-acid fermentation of saccharides by *Clostridium papyrosolvens*. Geochim. Cosmochim. Acta 70 (9), 2283–2297.
Planavsky, N.J., McGoldrick, P., Scott, C.T., Li, C., Reinhard, C.T., Kelly, A.E., Chu, X., Bekker, A., Love, G.D., Lyons, T.W., 2011. Widespread iron-rich conditions in the mid-Proterozoic ocean. Nature 477 (7365), 448–451.
Planavsky, N.J., Bekker, A., Hofmann, A., Owens, J.D., Lyons, T.W., 2012. Sulfur record of rising and falling marine oxygen and sulfate levels during the Lomagundi event. Proc. Natl. Acad. Sci. 109 (45), 18300–18305.
Planavsky, N.J., Asael, D., Hofmann, A., Reinhard, C.T., Lalonde, S.V., Knudsen, A., Wang, X., Ossa, F.O., Pecoits, E., Smith, A.J., Beukes, N.J., 2014. Evidence for oxygenic photosynthesis half a billion years before the great oxidation event. Nat. Geosci. 7 (4), 283–286.
Poser, A., Vogt, C., Knöller, K., Ahlheim, J., Weiss, H., Kleinsteuber, S., Richnow, H.H., 2014. Stable sulfur and oxygen isotope fractionation of anoxic sulfide oxidation by two different enzymatic pathways. Environ. Sci. Technol. 48 (16), 9094–9102.
Preuß, A., Schauder, R., Fuchs, G., Stichler, W., 1989. Carbon isotope fractionation by autotrophic bacteria with three different CO_2 fixation pathways. Z. Naturforsch. C 44 (5–6), 397–402.
Price, M.N., Ray, J., Wetmore, K.M., Kuehl, J.V., Bauer, S., Deutschbauer, A.M., Arkin, A.P., 2014. The genetic basis of energy conservation in the sulfate-reducing bacterium *Desulfovibrio alaskensis* G20. Front. Microbiol. 5, 577.
Quandt, L., Gottschalk, G., Ziegler, H., Stichler, W., 1977. Isotope discrimination by photosynthetic bacteria. FEMS Microbiol. Lett. 1 (3), 125–128.
Rabus, R., Hansen, T., Widdel, F., 2007. Dissimilatory sulfate- and sulfur-reducing prokaryotes. In: The Prokaryotes. Springer-Verlag, New York, pp. 659–768 Dworkin M.
Rasmussen, B., Bekker, A., Fletcher, I.R., 2013. Correlation of Paleoproterozoic glaciations based on U–Pb zircon ages for tuff beds in the Transvaal and Huronian Supergroups. Earth Planet. Sci. Lett. 382, 173–180.
Reinhard, C.T., Planavsky, N.J., Lyons, T.W., 2013. Long-term sedimentary recycling of rare sulphur isotope anomalies. Nature 497 (7447), 100–103.
Roberts, N.M., 2013. The boring billion?–Lid tectonics, continental growth and environmental change associated with the Columbia supercontinent. Geosci. Front. 4 (6), 681–691.
Rogers, J.J.W., Santosh, M., 2003. Supercontinents in Earth history. Gondwana Res. 6, 357–368.
Roth, A.S., Bourdon, B., Mojzsis, S.J., Rudge, J.F., Guitreau, M., Blichert-Toft, J., 2014. Combined^{147,146}Sm-^{143,142}Nd constraints on the longevity and residence time of early terrestrial crust. Geochem. Geophys. Geosyst. 15 (6), 2329–2345.
Rother, D., Henrich, H.J., Quentmeier, A., Bardischewsky, F., Friedrich, C.G., 2001. Novel genes of the sox gene cluster, mutagenesis of the Flavoprotein SoxF, and evidence for a general sulfur-oxidizing system in *Paracoccus* pantotrophusGB17. J. Bacteriol. 183 (15), 4499–4508.
Rudnicki, M.D., Elderfield, H., Spiro, B., 2001. Fractionation of sulfur isotopes during bacterial sulfate reduction in deep ocean sediments at elevated temperatures. Geochim. Cosmochim. Acta 65 (5), 777–789.
Rye, R., Holland, H.D., 1998. Paleosols and the evolution of atmospheric oxygen: a critical review. Am. J. Sci. 298 (8), 621–672.
Schidlowski, M., 2001. Carbon isotopes as biogeochemical recorders of life over 3.8 Ga of Earth history: evolution of a concept. Precambrian Res. 106 (1), 117–134.
Schidlowski, M., Hayes, J.M., Kaplan, I.R., 1983. Isotopic inferences of ancient biochemistries-Carbon, sulfur, hydrogen, and nitrogen. In: Schopf, J.W. (Ed.), Earth's Earliest Biosphere: Its Origin and Evolution. Princeton University Press, Princeton, NJ, pp. 149–186 (Print).
Schidlowski, M., Gorzawski, H., Dor, I., 1994. Carbon isotope variations in a solar pond microbial mat: role of environmental gradients as steering variables. Geochim. Cosmochim. Acta 58 (10), 2289–2298.
Schmidt, T.M., Arieli, B., Cohen, Y., Padan, E., Strohl, W.R., 1987. Sulfur metabolism in Beggiatoa alba. J. Bacteriol. 169, 5466–5472.
Schopf, J.W., 1974. The development and diversification of Precambrian life. Orig. Life 5 (1–2), 119–135.
Schrag, D.P., Higgins, J.A., Macdonald, F.A., Johnston, D.T., 2013. Authigenic carbonate and the history of the global carbon cycle. Science 339 (6119), 540–543.
Scott, C., Wing, B.A., Bekker, A., Planavsky, N.J., Medvedev, P., Bates, S.M., Yun, M., Lyons, T.W., 2014. Pyrite multiple-sulfur isotope evidence for rapid expansion and contraction of the early Paleoproterozoic seawater sulfate reservoir. Earth Planet. Sci. Lett. 389, 95–104.
Shields, G., Veizer, J., 2002. Precambrian marine carbonate isotope database: version 1.1. Geochem. Geophys. Geosyst. 3 (6).
Shock, E.L., Holland, M., Meyer-Dombard, D.R., Amend, J.P., 2005. Geochemical sources of energy for microbial metabolism in hydrothermal ecosystems: Obsidian Pool, Yellowstone National Park. In: Inskeep, W., McDermott, T. (Eds.), Geothermal Biology and Geochemistry in Yellowstone National Park: Proceeding of the Thermal Biology Institute Workshop, Yellowstone National Park, WY, October 2003. Montana State University Publications, pp. 95–112.
Sim, M.S., Bosak, T., Ono, S., 2011. Large sulfur isotope fractionation does not require disproportionation. Science 333 (6038), 74–77.
Sirevåg, R., Buchanan, B.B., Berry, J.A., Troughton, J.H., 1977. Mechanisms of CO_2 fixation in bacterial photosynthesis studied by the carbon isotope fractionation technique. Arch. Microbiol. 112 (1), 35–38.
Slack, J.F., Cannon, W.F., 2009. Extraterrestrial demise of banded iron formations 1.85 billion years ago. Geology 37 (11), 1011–1014.
Sleep, N.H., Bird, D.K., 2007. Niches of the pre-photosynthetic biosphere and geologic preservation of Earth's earliest ecology. Geobiology 5 (2), 101–117.
Smith, E., Morowitz, H.J., 2004. Universality in intermediary metabolism. Proc. Natl. Acad. Sci. U. S. A. 101 (36), 13168–13173.
Sun, C.W., Chen, Z.W., He, Z.G., Zhou, P.J., Liu, S.J., 2003. Purification and properties of the sulfur oxygenase/reductase from the acidothermophilic archaeon, *Acidianus* strain S5. Extremophiles 7 (2), 131–134.
Swanner, E.D., Wu, W., Hao, L., Wüstner, M.L., Obst, M., Moran, D.M., McIlvin, M.R., Saito, M.A., Kappler, A., 2015. Physiology, Fe(II) oxidation, and Fe mineral formation by a marine planktonic cyanobacterium grown under ferruginous conditions. Front. Earth Sci. 3, 60.
Takai, K., Nakamura, K., Toki, T., Tsunogai, U., Miyazaki, M., Miyazaki, J., Hirayama, H., Nakagawa, S., Nunoura, T., Horikoshi, K., 2008. Cell proliferation at 122 °C and isotopically heavy CH_4 production by a hyperthermophilic methanogen under high-pressure cultivation. Proc. Natl. Acad. Sci. 105 (31), 10949–10954.

Tang, M., Chen, K., Rudnick, R.L., 2016. Archean upper crust transition from mafic to felsic marks the onset of plate tectonics. Science 351 (6271), 372–375.
Taylor, S.R., McLennan, S.M., 1995. The geochemical evolution of the continental crust. Rev. Geophys. 33 (2), 241–265.
Thompson, J.B., Ferris, F.G., Smith, D.A., 1990. Geomicrobiology and sedimentology of the mixolimnion and chemocline in Fayetteville Green Lake, New York. PALAIOS 52–75.
Ueno, Y., Ono, S., Rumble, D., Maruyama, S., 2008. Quadruple sulfur isotope analysis of ca. 3.5 Ga Dresser Formation: new evidence for microbial sulfate reduction in the early Archean. Geochim. Cosmochim. Acta 72 (23), 5675–5691.
Valentine, D.L., Chidthaisong, A., Rice, A., Reeburgh, W.S., Tyler, S.C., 2004. Carbon and hydrogen isotope fractionation by moderately thermophilic methanogens. Geochim. Cosmochim. Acta 68 (7), 1571–1590.
van der Meer, M.T., Schouten, S., Rijpstra, W.I.C., Fuchs, G., Damsté, J.S.S., 2001. Stable carbon isotope fractionations of the hyperthermophilic crenarchaeon *Metallosphaera sedula*. FEMS Microbiol. Lett. 196 (1), 67–70.
Van Gemenden, H., Mas, J., 1995. Ecology of phototrophic sulfur bacteria. In: Blankenship, R.E., Madigan, M.T., Bauer, C. (Eds.), Anoxygenic Photosynthetic Bacteria. Springer-Verlag, New York, NY, pp. 49–85.
Van Houten, F.B., 1973. Origin of red beds: a review-1961–1972. Annu. Rev. Earth Planet. Sci. 1, 39.
Wächtershäuser, G., 1990. Evolution of the first metabolic cycles. Proc. Natl. Acad. Sci. 87 (1), 200–204.
Walker, J.C., 1977. Evolution of the Atmosphere. 1977. Collier Macmillan, New York: Macmillan, and London, pp. 1.
Walter, X.A., 2011. Anaerobic Iron Cycling in a Neoarchean Ocean Analogue. University of Neuchâtel, Switzerland (Ph.D. thesis).
Walter, X.A., Picazo, A., Miracle, M.R., Vicente, E., Camacho, A., Aragno, M., Zopfi, J., 2014. Phototrophic Fe(II)-oxidation in the chemocline of a ferruginous meromictic lake. Front. Microbiol. 5, 713.
Watanabe, Y., Farquhar, J., Ohmoto, H., 2009. Anomalous fractionations of sulfur isotopes during thermochemical sulfate reduction. Science 324 (5925), 370–373.
Whitehill, A.R., Xie, C., Hu, X., Xie, D., Guo, H., Ono, S., 2013. Vibronic origin of sulfur mass-independent isotope effect in photoexcitation of SO_2 and the implications to the early earth's atmosphere. Proc. Natl. Acad. Sci. 110 (44), 17697–17702.
Whiticar, M.J., 1999. Carbon and hydrogen isotope systematics of bacterial formation and oxidation of methane. Chem. Geol. 161 (1), 291–314.
Wille, M., Kramers, J.D., Nägler, T.F., Beukes, N.J., Schröder, S., Meisel, T., Lacassie, J.P., Voegelin, A.R., 2007. Evidence for a gradual rise of oxygen between 2.6 and 2.5 Ga from Mo isotopes and Re-PGE signatures in shales. Geochim. Cosmochim. Acta 71 (10), 2417–2435.
Wolf, E.T., Toon, O.B., 2010. Fractal organic hazes provided an ultraviolet shield for early Earth. Science 328 (5983), 1266–1268.
Wortmann, U.G., Bernasconi, S.M., Böttcher, M.E., 2001. Hypersulfidic deep biosphere indicates extreme sulfur isotope fractionation during single-step microbial sulfate reduction. Geology 29 (7), 647–650.
Xiao, S., Dong, L., 2006. On the morphological and ecological history of Proterozoic macroalgae. In: Neoproterozoic Geobiology and Paleobiology. Springer, Netherlands, pp. 57–90.
Young, G.M., 2013. Precambrian supercontinents, glaciations, atmospheric oxygenation, metazoan evolution and an impact that may have changed the second half of Earth history. Geosci. Front. 4 (3), 247–261.
Young, G.M., Brunn, V.V., Gold, D.J., Minter, W.E.L., 1998. Earth's oldest reported glaciation: physical and chemical evidence from the Archean Mozaan Group (~2.9 Ga) of South Africa. J. Geol. 106 (5), 523–538.
Zahnle, K., Claire, M., Catling, D., 2006. The loss of mass-independent fractionation in sulfur due to a Palaeoproterozoic collapse of atmospheric methane. Geobiology 4 (4), 271–283.
Zeebe, R.E., Wolf-Gladrow, D.A., 2001. CO_2 in Seawater: Equilibrium, Kinetics, Isotopes (No. 65). Gulf Professional Publishing.
Zhelezinskaia, I., Kaufman, A.J., Farquhar, J., Cliff, J., 2014. Large sulfur isotope fractionations associated with Neoarchean microbial sulfate reduction. Science 346 (6210), 742–744.